

The Anisotropic Distribution of Satellite Galaxies

Jeremy Bailin^{1,2}, Chris Power¹, Peder Norberg^{3,4}, Dennis Zaritsky⁵, Brad K. Gibson⁶

¹Centre for Astrophysics and Supercomputing, Swinburne University of Technology, Mail H39, PO Box 218, Hawthorn, Victoria, 3122, Australia; (jbailin, cpower)@astro.swin.edu.au

²Current address: Department of Physics & Astronomy, ABB-241, McMaster University, 1280 Main St. W, Hamilton, ON, L8S 4M1, Canada

³The Royal Observatory Edinburgh, Blackford Hill, Edinburgh, EH9 3HJ, UK; iprn@roe.ac.uk

⁴ETHZ Institut für Astronomie, HPF G3.1, ETH Hönggerberg, CH-8093 Zürich, Switzerland

⁵Steward Observatory, University of Arizona, 933 North Cherry Ave, Tucson, AZ, 85721; dzaritsky@as.arizona.edu

⁶Centre for Astrophysics, University of Central Lancashire, Preston PR1 2HE; bkgibson@uclan.ac.uk

4 December 2021

ABSTRACT

Contrary to several recent studies, we find strong evidence in the Sloan Digital Sky Survey for the “Holmberg Effect”, the tendency for the satellites of isolated late-type galaxies to align with the *minor axis* of the galactic disc. In the case of isolated early-types, we find that satellites tend to align with the *major axis* of the galaxy. Using mock catalogues generated from cosmological N -body simulations, we demonstrate that previous studies, which found results to the contrary, used galaxy samples that were dominated by the members of galaxy groups rather than isolated galaxies. If we duplicate the selection criteria of these studies, we recover their results: namely, group members tend to cluster along the major axis of the brightest group galaxy if it is an early-type, but are distributed isotropically if it is a late-type. We find strong evidence for an anisotropic satellite distribution out to $350 h^{-1} \text{ kpc}$ around isolated late-types and $500 h^{-1} \text{ kpc}$ around isolated early-types. It is interesting to note that the polar alignment we detect around external late-types has the same sign and magnitude as the alignment of satellites around the major Local Group spirals. Our analysis suggests that satellites at large projected radii show a slight tendency to lie along the same axis as the surrounding large scale structure. We discuss the origin of the anisotropic satellite distribution and we consider the implications of our results, critically assessing the respective roles played by dynamical evolution of satellite orbits; anisotropic accretion of satellites from the larger scale environment; and the biased nature of satellites as tracers of the underlying dark matter subhalo population.

Key words: galaxies: haloes — dark matter — galaxies: structure — galaxies: dwarf — galaxies: clusters: general — galaxies: formation

1 INTRODUCTION

The spatial distribution of satellites around isolated galaxies can provide important insights into the mass distribution in and around these galaxies. If dynamical effects could be neglected and if we could assume that satellite galaxies inhabit an unbiased set of dark matter subhaloes, then we would expect satellites to cluster preferentially along the major axis of the host dark matter halo of the primary galaxy, as in galaxy cluster mass haloes (Knebe et al. 2004). We could therefore determine the orientation of the parent galaxy within its dark matter halo by using the spatial distribution of its satellite galaxies.

However, there is good reason to believe that dynamical effects will play an important role in determining the spatial distribution of satellites. For example, Hartwick (2000) has argued that the imprint of anisotropic infall of satellites

along filaments is evident in the orbits of recently accreted systems, and Peñarrubia et al. (2002) have shown that the inclination of a satellite’s orbit can determine its dynamical response to the disc or spheroid of its parent galaxy. There is also good reason to suspect that the relationship between satellites and the underlying dark matter subhalo population may not be straightforward, as has been argued by, for example, Gao et al. (2004) (but see Conroy et al. 2006). Indeed, current galaxy formation models indicate that satellite galaxies represent a biased subset of subhaloes whose spatial distribution is very likely to be anisotropic within their parent galaxy’s dark matter halo (e.g. Zentner et al. 2005; Libeskind et al. 2005).

These considerations suggest that interpretation of the spatial distribution of satellites may be more complex than we might naively expect. Yet, despite these complexities,

satellite galaxies represent a powerful observational probe into the mass distribution around galaxies. Therefore, it is essential to determine robustly the spatial distribution of satellite galaxies, and to establish whether or not they show a preferential alignment relative to their parent galaxies. This is the aim of the current study.

Locally we see strong evidence for the preferential alignment or *anisotropic distribution* of satellites relative to their primary galaxies. Both the Milky Way and M31 have satellite populations that lie in great planes that are highly inclined to their discs. This has been noted by Lynden-Bell (1976), Hartwick (2000) and Kroupa et al. (2005) for the Milky Way; by Koch & Grebel (2006) and McConnachie & Irwin (2006) for M31; and by Metz et al. (2007), who performed an analysis of the statistical significance of the planar distribution around both galaxies. The Milky Way and M31 are the only galaxies for which the sample of satellites is large enough that their spatial distribution is analysed directly (without requiring stacking to obtain a statistical sample). They are also the only systems for which we are certain that the satellites are physically associated with their primaries, and for which the three-dimensional positions of the satellites with respect to their primaries are known. In addition, proper motion measurements exist for a number of Milky Way satellites, which confirm that these systems are on polar orbits (Palma et al. 2002).

Analysing the spatial distribution of satellites in external systems is generally more challenging because no more than one or two satellites are detected per primary galaxy. This measurement requires that primaries and their satellites be stacked to obtain statistical samples from which the angular distribution of satellites about a “typical” primary is determined. Such an analysis was first performed by Holmberg (1969) for 58 isolated spiral or *late-type* galaxies and their 218 optical companions, of which 75 were expected to be physically associated. He found that satellites at projected radii less than 50 kpc were more often found near the poles (minor axis) of the primary’s disc (Figure 1). This preferential polar distribution, referred to as the “Holmberg Effect”, was subsequently confirmed by Zaritsky et al. (1997b) (hereafter ZSFW) at larger projected radii of 300 – 500 kpc using a sample of 115 spectroscopically-confirmed satellite galaxies of 69 isolated late-types.

The advent of large galaxy redshift surveys such as the 2dF Galaxy Redshift Survey (2dFGRS; Colless et al. 2001) and the Sloan Digital Sky Survey (SDSS; York et al. 2000) has enabled this issue to be revisited. These surveys provide an abundance of galaxies with spectroscopic redshifts, and several recent studies have sought to use numbers of galaxies far in excess of those that were available to Holmberg (1969) and ZSFW to address the question of spatial anisotropy with *significantly improved statistics*. Sales & Lambas (2004) (hereafter SL04) used over 2000 satellites of almost 1500 primary galaxies in the 2dFGRS, and found that satellites around blue primaries tended to follow an isotropic distribution, whereas those around red primaries tended to align with the *major-axis*. This finding contrasts sharply with the polar distribution inferred by

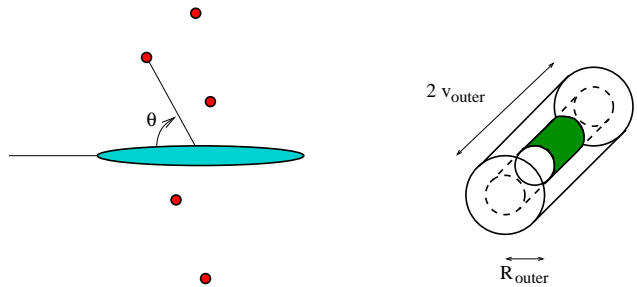


Figure 1. (Left) The Holmberg Effect: satellites of disc galaxies tend to lie near the minor axis of the disc. This corresponds to an angle between the major axis of the galaxy and the satellite (the “disc angle”, θ) of greater than 45° . (Right) Selection cylinders around a potential primary galaxy, which lies at the centre of the cylinders. The outer isolation cylinder is marked with solid lines and has radius R_{outer} and length $2v_{\text{outer}}$. The inner isolation cylinder is marked with dashed lines and has radius R_{inner} and length $2v_{\text{inner}}$. The satellites are drawn from the shaded cylinder with radius R_{sat} and length $2v_{\text{sat}}$.

both Holmberg (1969) and ZSFW¹. Yang et al. (2006) (hereafter Y06), Azzaro et al. (2007) (hereafter APPZ) and Agustsson & Brainerd (2007) (hereafter AB07) detected the same effect in the SDSS; Y06 used over 16000 groups of galaxies selected to lie within the same dark matter halo, while APPZ and AB07 studied satellites of isolated galaxies; intriguingly, the latter study found that the isotropic distribution around blue galaxies was composed of a *major-axis* alignment for satellites at small projected radii and a *minor-axis* alignment for satellites at large projected radii. Brainerd (2005) (hereafter B05) also selected satellites of isolated galaxies in the SDSS (her largest sample contained approximately 3000 satellites around 2000 primaries) and found that they exhibited a major-axis distribution. A similar result was obtained by Faltenbacher et al. (2007), who examined members of over 18000 groups in the SDSS. Finally, Azzaro et al. (2006) (hereafter AZPK) found no evidence for anisotropy based on a smaller sample of 193 satellites of 144 isolated late-type galaxies in the SDSS.

These results, derived from both 2dFGRS and SDSS, would seem to suggest that the preferential alignment of satellites about the poles of their primaries noted by both Holmberg (1969) and ZSFW was a consequence of small number statistics. However, the spatial anisotropy reported by ZSFW was detected with a statistical confidence greater than 99%, suggesting that small number statistics were unlikely to be a problem. Furthermore, as we have noted already, there is strong evidence for the preferential alignment of satellites about the poles of both the Milky Way and M31, systems for which we can be certain that we know that the satellites are physically associated with their primaries and for which we know their spatial distribution. Both of these observations indicate that it is systematic rather than random errors that more strongly affect detection of spatial anisotropies in the distribution of satellites around external galaxies. This leads us to the issue of sample selection.

¹ We note that this is opposite to the original claims of SL04; see the discussion in Y06 for further details

In the case of both the Milky Way and M31, we have an abundance of detailed information that allows us to state with confidence which galaxies can be considered satellites belonging to these hosts. In the case of external galaxies, we do not have such detailed information and so we must employ selection criteria that allow us to identify which faint galaxy neighbours in projection are likely to be satellites of the primary. Differences arising from how satellite galaxies are selected will affect measurements of the angular distribution of satellites, and will therefore influence how these data are interpreted.

To illustrate this point, we know that the member galaxies of groups and clusters tend to cluster about the major axis of the Brightest Group or Cluster Galaxy (BGG and BCG respectively; e.g. Binggeli 1982; West 1989; Mandelbaum et al. 2006). If we identify these group or cluster members as satellites of their primary galaxy, the BGG or BCG, then we would interpret this measurement as showing that group or cluster members preferentially align with their primary’s major-axis. However, we do not expect groups or clusters to be dynamically relaxed and so satellites in these systems are unlikely to trace the potential of an equilibrium mass distribution. Therefore, the study of satellites around *isolated* galaxies must be highly successful at excluding such groups and clusters. The ability of selection criteria to identify the proper type of system and to suppress contamination is essential for the result to be considered robust and physical.

Mock galaxy catalogues constructed from cosmological N -body simulations provide a powerful method for assessing the reliability of selection criteria. Dark matter haloes are populated with mock galaxies following either a statistical approach based on “Halo Occupation Distributions” (HOD; e.g. Berlind & Weinberg 2002), or a physically motivated approach based on semi-analytical galaxy formation models (e.g. Cole et al. 2000). Both approaches are parameterised and so statistical properties of the mock galaxy population, such as the luminosity function and the 2-point correlation function, are fine-tuned to recover the observed properties of real galaxies in the 2dFGRS and the SDSS. This provides an ideal testbed for selection criteria. We adopt the “Conditional Luminosity Function” (CLF) formalism of Yang et al. (2003), a statistical approach based on HODs, to develop our suite of mock catalogues. The CLF formalism allows us to assign to each dark matter halo in a cosmological N -body simulation a probability of hosting N galaxies with a total luminosity L , and a distribution of luminosities drawn from a Schechter function whose parameters depend on the halo mass M . Further details are presented in § 2.3.

We note that previous studies have used mock galaxy catalogues derived from the CLF formalism to investigate the radial distribution (van den Bosch et al. 2005) and kinematics (van den Bosch et al. 2004) of satellite galaxies. However, we use our mock catalogues to establish *optimal selection criteria* that preferentially pick out *isolated systems* of primary galaxies and their satellites. We explore the impact of different selection criteria on the nature of satellite samples (e.g. group or cluster members?) and to establish robust criteria that minimise the influence of interlopers and a primary’s larger-scale environment. This allows us to assess selection criteria adopted in previous

studies and to quantify the ability of these criteria to identify isolated systems.

By taking such care in establishing the criteria by which our isolated systems are selected, we are able to address a number of important outstanding physical questions using a *robust* sample of galaxies taken from the SDSS. In particular, we revisit the question of whether or not the angular distribution of satellite galaxies about their primary is anisotropic, and whether or not anisotropy is linked to the morphological type of the primary. Such a dependence would present an exciting possibility to study the connection between subhaloes, haloes, and galaxy morphology. In § 5 we discuss the physical significance of our results in this context.

We note also natural overlaps with studies that seek to measure the flattening of dark matter haloes. There is good evidence to suggest that the haloes of early-type galaxies are flattened along the minor axis of the light – based on studies of X-ray isophotes (e.g. Buote et al. 2002) and weak lensing (e.g. Hoekstra et al. 2004) – whereas the results for disc galaxies are inconclusive. For example, the tidal stream of the Sagittarius Dwarf has been used to infer that the Milky Way’s halo is spherical (Ibata et al. 2001), flattened in the same sense as the disc (Martínez-Delgado et al. 2004; Johnston et al. 2005), or flattened in the opposite sense as the disc (Helmi 2004), depending on which part of the stream is modelled (Law et al. 2005). We discuss the implications of our results for halo flattening in § 5.

The structure of this paper is as follows: in § 2 we discuss the sample selection criteria, and present our sample of satellites of isolated galaxies. In § 3 we present our results for the anisotropic distribution of satellite galaxies with respect to their primary galaxy and to large scale filaments. In § 4 we analyze the differences between our conclusions and those of previous authors and use the mock catalogues to demonstrate that this difference is due mainly to the different selection criteria. Finally, we discuss the interpretation of the results in terms of the shapes of dark matter haloes, anisotropic infall, unrelaxed groups, and the formation of galactic discs in § 5.

2 SAMPLE SELECTION

The most critical part of the analysis is the process of selecting satellite galaxies of isolated primaries. We must simultaneously:

- (i) Minimize the number of primaries that are not isolated, i.e. which do not dominate the dynamics of their environment.
- (ii) Minimize the number of “interlopers”, or satellite-primary pairs that do not represent physical satellites of the primary galaxy.
- (iii) Maximize the sample size, subject to the above constraints.

We use mock catalogues generated from cosmological simulations to refine our criteria to fulfil the above requirements and to critically examine the selection criteria that have been used in previous studies.

2.1 Observational Data

2.1.1 Sloan Digital Sky Survey

Our sample is drawn from the Sloan Digital Sky Survey Data Release 5 (SDSS DR5) (Adelman-McCarthy et al. 2007). All primary survey objects classified as galaxies in the imaging data that satisfy the spectroscopic targeting algorithm of either the Main galaxy sample (Strauss et al. 2002) or the Luminous Red Galaxy sample (Eisenstein et al. 2001) are considered. Only galaxies with valid spectroscopic redshifts (sciencePrimary = 1 and zConf > 0.35) that are also spectroscopically classified as galaxies are considered as primary or satellite galaxies; however, galaxies without such spectra are also used when evaluating the isolation criteria. Petrosian magnitudes are used throughout, and are dereddened using the corrections in Schlegel et al. (1998) and k-corrected using KCORRECT v4.1.4 (Blanton et al. 2003) to the $^{0.1}r$ band² to minimize the effect of errors in the k-correction. The nominal survey limit for spectroscopic targets in the SDSS Main galaxy sample is $r \leq 17.77$; however, the actual limit varies across the sky. Therefore, we conservatively treat it as only being complete to $r \leq 17.5$, although we make use of galaxies as faint as $r = 17.77$ when they are available. When we require photometric redshifts, we use the neural network photometric redshifts available in the SDSS DR5 catalogue. Angular diameter distances and distance moduli are calculated assuming $\Omega_m = 0.3$ and $\Omega_\Lambda = 0.7$ and are quoted in h -independent units, where $H_0 = h \, 100 \, \text{km s}^{-1} \, \text{kpc}^{-1}$.

2.1.2 Galaxy Classification

It is important to separate spheroid-dominated early-type galaxies from disc-dominated late-type galaxies. The major axes of early-type galaxies are determined by their anisotropic velocity dispersions while those of late-type galaxies are determined by their angular momentum; therefore, their orientation with respect to the dark matter halo may be different. Furthermore, the dynamical effects of discs versus spheroids on satellite orbits may be different. Indeed, many previous studies have found that the satellites around red and blue galaxies are distributed differently.

We classify galaxies using a linear combination of three independent parameters: the location on the colour-magnitude diagram, the spectroscopic Principal Component Analysis, and the global concentration of the light profile. Details of the classification scheme and an analysis of the results when other classification schemes are adopted are given in Appendix C. We find that our qualitative results are unchanged for any reasonable method of splitting the sample, although the numerical magnitude of the effect can vary by $\sim 1\sigma$ depending on the classification method.

2.2 Definition of Selection Criteria

The format of our selection criteria is based on Norberg et al. (2007) and is similar to that used in previous studies; however, the details differ in several important

ways. To be considered isolated, primaries must not have any comparably bright neighbours within a large surrounding region, and must be much brighter than all potential satellites in the immediate vicinity. We define three cylinders around each potential primary (see Figure 1):

- Outer isolation cylinder: All galaxies within a projected separation of $\Delta R \leq R_{\text{outer}}$ and a velocity difference of $|\Delta v| \leq v_{\text{outer}}$ must be at least m_{outer} magnitudes fainter in r .
- Inner isolation cylinder: All galaxies within a projected separation of $\Delta R \leq R_{\text{inner}}$ and a velocity difference of $|\Delta v| \leq v_{\text{inner}}$ must be at least m_{inner} magnitudes fainter in r ($m_{\text{inner}} > m_{\text{outer}}$).
- Satellite cylinder: Satellites are galaxies within a projected separation of $\Delta R \leq R_{\text{sat}}$ and a velocity difference of $|\Delta v| \leq v_{\text{sat}}$. Satellites must be at least m_{sat} magnitudes fainter in r . For our criteria, we enforce $R_{\text{sat}} = R_{\text{inner}}$, $m_{\text{sat}} = m_{\text{inner}}$, and $v_{\text{sat}} = \frac{1}{2}v_{\text{inner}}$.

The adopted values of the parameters are given in Table 1. To ensure that satellites are not associated with more than one primary (a situation we refer to as a “multi-homed” satellite) and that there are no near neighbours too luminous to be satellites, it is important that $R_{\text{inner}} \leq \frac{1}{2}R_{\text{outer}}$, $v_{\text{inner}} = v_{\text{outer}}$, $R_{\text{sat}} \leq R_{\text{inner}}$, $v_{\text{sat}} \leq \frac{1}{2}v_{\text{inner}}$, and $m_{\text{sat}} = m_{\text{inner}}$. These sanity checks are not fulfilled by many of the criteria that have been used in previous studies.

We also apply the following additional criteria:

(i) All primaries must be at least m_{inner} magnitudes brighter than $r = 17.5$ to ensure that all potential bright neighbours are brighter than the local survey limit.

(ii) The projected distance from the primary to the nearest edge of the photometric survey footprint must be at least R_{outer} to ensure that any potential bright neighbours have been observed photometrically. The projected distance from the primary to the nearest edge of the spectroscopic survey footprint must be at least R_{sat} to ensure that all potential satellites are equally likely to have been observed spectroscopically and therefore that the survey edge does not impose an angular bias in the selected satellite population.

(iii) Because of spectral incompleteness, $\sim 10\%$ of galaxies that fulfil the requirements of the SDSS Main galaxy targeting criteria do not have observed redshifts. Therefore, there are potential primaries that would not be considered isolated if it turned out that their non-spectroscopic neighbours are at the same redshift. This issue is particularly important because the limited number of fibres per tile causes the fractional completeness to be lower in regions of high galactic density. There are a number of ways of treating such galaxies: one could assume that most such neighbours do not lie at the same redshift as the primary and simply ignore their presence (SL04; B05; AZPK; APPZ; Y06; AB07), one could establish a threshold such that if there are more than a number N_{viol} of potential criteria-violating neighbours then the chances that at least one is at the same redshift as the primary is high and therefore eliminate those primaries (Norberg et al. 2007; Herbert-Fort et al., in preparation), or one could eliminate all such primaries on the grounds that there is a chance that they are not isolated (equivalent to setting $N_{\text{viol}} = 0$; ZSFW). The existence of photometric redshifts in the SDSS DR5 catalogue allows us

² The r band redshifted to $z = 0.1$; for simplicity we use the notation M_r to refer to $M_{0.1,r}$.

Table 1. Parameters of Selection Criteria

Parameter	This Work	ZSFW	SL04	S1	B05 S2	S3	AZPK	APPZ S1	S2	AB07
Outer isolation cylinder:										
$R_{\text{outer}} (h^{-1} \text{ kpc})$	1000	750	700
$v_{\text{outer}} (\text{km s}^{-1})$	1500	1000	1000
m_{outer}	0.7	0.7	0.7
Inner isolation cylinder:										
$R_{\text{inner}} (h^{-1} \text{ kpc})$	500	375	700	490	2000	350	500	490	500	511
$v_{\text{inner}} (\text{km s}^{-1})$	1500	1000	1000	1000	1000	1000	1000	1000	1000	1000
m_{inner}	2.0	2.2	1.0	1.0	0.7	2.2	2.0	1.0	2.0	1.0
Satellite cylinder:										
$R_{\text{sat}} (h^{-1} \text{ kpc})$	500	375	500	350	350	350	350	350	350	365
$v_{\text{sat}} (\text{km s}^{-1})$	750	500	500	500	1000	500	500	500	500	500
m_{sat}	2.0	2.2	2.0	2.0	1.5	2.2	2.0	2.0	2.0	2.0
N_{viol}	photo- z^e	0 ^e
f_{sat}	0.2	1.0	1.0	1.0	1.0
N_{satmax}	4	...	4	9
Sanity checks:										
Forbids multi-homed satellites ^a	Yes	Yes	No	No	No	Yes	Yes	No	Yes	No
Forbids nearby non-satellites ^b	Yes	Yes	No	No	No	Yes	Yes	No	Yes	No
Avoids survey edge ^c	Yes	N/A	No	No	No	No	Yes ^e	No	No	Yes
Avoids survey magnitude limit ^d	Yes	Yes	No	No	No	No	Yes	No	Yes	No

^aThe criteria do not permit satellites to belong to more than one primary galaxy.

^bThe criteria do not permit there to be bright (non-satellite) galaxies within the satellite cylinder.

^cThe criteria do not permit primaries so near the edge of the survey that potential bright neighbours would lie outside the survey region.

^dThe criteria do not permit primaries faint enough that potential bright neighbours fall below the local survey magnitude limit.

^eSee text for further clarification.

to use a more sophisticated method of determining whether these potential isolation criteria violators are likely to be at the same redshift as the primary: if the photometric redshift of the neighbour $z_{\text{viol,photo}}$ is within $2\sigma_{\text{viol,photo}}$ of the spectroscopic redshift of the primary, where $\sigma_{\text{viol,photo}}$ is the estimated error on the photometric redshift in the catalogue, then we eliminate the primary. We ignore the presence of potential violators that have unreliable photometric redshifts (flag = 1 or flag = 3) or do not exist in the photometric redshift database as these are mostly galaxies that are not detected in one or more bands; such galaxies are highly unlikely to be truly bright physical neighbours of the relatively luminous nearby galaxies that constitute our sample of primary galaxies. We have confirmed that excluding primaries with such neighbours does not alter our conclusions.

(iv) The total luminosity of the satellites must not be more than f_{sat} times the luminosity of the primary, and systems with more than N_{satmax} satellites are discarded. This ensures that the primary galaxy dominates the satellite system.

(v) Postage stamp images of each potential primary were examined by eye. 6 objects were removed, 3 of which suffered from catastrophically bad background subtraction due to nearby bright objects and 3 of which are major mergers in progress.

Our choices for the relevant parameters are motivated by analysis using mock catalogues as described in § 2.3.4. Where applicable, the values previous authors have used for the selection parameters are given in Table 1. For those cri-

teria that use only one isolation cylinder, we characterize it as an “Inner” cylinder. We summarize the selection criteria used by each previous study below:

ZSFW used somewhat thinner and shorter cylinders than those used in this work, but the criteria fulfil the above sanity checks. They did not have redshifts and magnitudes for every galaxy in the field, but eliminated all primaries that appeared by eye to have potentially criteria-violating neighbours (i.e. $N_{\text{viol}} = 0$). There was no formal edge of the surveyed area, and primaries were chosen to be at least 2.5 mag brighter than the POSS magnitude limit, so all potential bright neighbours were considered. No cut on the number or luminosity fraction of satellites was imposed, and only morphological late-types were included as primaries.

SL04 used only one isolation cylinder, which did not satisfy $m_{\text{sat}} \leq m_{\text{outer}}$. Therefore, relatively bright galaxies are allowed to be in the satellite region. Because of this definition, satellites may be multi-homed. Only primary galaxies with absolute magnitude $M_{\text{bj}} - 5 \log h < -18$ were used. They did not impose any constraints on proximity to the survey magnitude limit, proximity to the survey edge, N_{viol} , or f_{sat} , but used $N_{\text{satmax}} = 4$.

B05 tested three selection criteria; her Sample 1 (S1) used isolation criteria based on SL04 (though adopting a different value of the Hubble constant); her Sample 2 (S2) used one very wide isolation cylinder, which permits bright galaxies to be in the satellite region and satellites to be multi-homed; and her Sample 3 (S3) used isolation criteria based on ZSFW (though adopting a different value of the Hubble constant). There was no cut on proximity to the

survey edge, N_{viol} , or N_{satmax} in any of the samples. There was a cut on f_{sat} of 1.0.

AZPK used Sample 2 of Prada et al. (2003), but restricted the primaries to be morphological late-types, adopted a redshift limit of $cz \leq 11000 \text{ km s}^{-1}$, and only examined primaries with $-20.5 \leq M_B \leq -19.5$. These criteria are similar to SL04, except that because $m_{\text{sat}} = m_{\text{outer}}$, the satellite cylinder is not permitted to contain bright galaxies and satellites can only belong to a single primary. Although they did not formally adopt a cut on proximity to the survey edge, they searched for bright neighbours in de Vaucouleurs et al. (1991) (RC3), which fulfils the same purpose. The narrow range of absolute magnitudes and redshift limit serve the same purpose as our cut on galaxies near the survey magnitude limit. They did not make any cut on N_{viol} , N_{satmax} , or f_{sat} .

APPZ tested two sets of criteria. Their Sample 1 (S1) uses the same criteria as B05 S1 but without the cut on f_{sat} . Their Sample 2 (S2) is identical to AZPK except that a wider range of primary luminosities, $-23 \leq M_r \leq -21$ is used, the redshift limit is extended to $cz \leq 30000 \text{ km s}^{-1}$, and no check for bright neighbours outside of the survey boundary is performed.

AB07 used criteria very similar to B05 S1, but they adopted a slightly different value for the Hubble constant, restricted N_{satmax} to 9, and ensured that their primary galaxies were not near the edge of the spectroscopic survey.

Holmberg (1969) did not have redshifts for any of his galaxies, making it difficult to directly compare our selection. It is also difficult to compare our selection with Y06 or Faltenbacher et al. (2007), who used an iterated percolation algorithm rather than isolation criteria. Their selections were tuned using mock catalogues to minimize the number of interlopers; however, they were not designed to find isolated galaxies and most of their systems should be considered groups or clusters rather than satellite systems of isolated galaxies.

Our criteria are more restrictive than other criteria that have been used to select isolated galaxies. The advantage of using such a large sample as SDSS DR5 is less the ability to boost the statistics than the ability to be extremely conservative with our selection criteria and still retain an acceptable number of galaxies. Given that the disagreement between previous results is more likely due to systematic errors than statistics, such a rigorous treatment is essential to disentangling the nature of the disagreement and determining the true distribution.

2.3 Mock Catalogues

2.3.1 The Conditional Luminosity Function $\Phi(L|M)$

We construct our mock galaxy catalogues following the prescription presented in Yang et al. (2004) (hereafter Y04), which is based on earlier studies by Yang et al. (2003) and van den Bosch et al. (2003). This approach allows us to assign to each dark matter halo of mass M a probability of hosting a population of N galaxies of total luminosity L . This probability is governed by the “Conditional Luminosity Function”, $\Phi(L|M)$, which is parameterised by the Schechter function,

Table 2. Cosmological N -body Simulations. L_{box} refers to the length of the simulation box; m_{part} is the particle mass, which depends on both L_{box} and the number of particles N_{part} ; ϵ is the gravitational force softening; M_{min} is a (conservative) estimate of minimum halo mass that can be reliably resolved, based on convergence of the mass function; and L_{min} is the minimum luminosity.

L_{box} [$h^{-1}\text{Mpc}$]	m_{part} [$h^{-1}M_{\odot}$]	ϵ [$h^{-1}\text{kpc}$]	M_{min} [$h^{-1}M_{\odot}$]	L_{min} [$h^{-2}L_{\odot}$]
35	0.21×10^9	2.7	10^{10}	1.1×10^8
50	0.62×10^9	3.9	3×10^{10}	1.1×10^8
70	1.7×10^9	5.5	9×10^{10}	1.1×10^9
100	4.96×10^9	7.8	25×10^{10}	1.1×10^9

$$\Phi(L|M)dL = \frac{\tilde{\Phi}^*}{\tilde{L}^*} \left(\frac{L}{\tilde{L}^*} \right)^{\tilde{\alpha}} \exp(-L/\tilde{L}^*) dL. \quad (1)$$

The normalisation $\tilde{\Phi}^*$, characteristic luminosity \tilde{L}^* , and faint-end slope $\tilde{\alpha}$ are all functions of halo mass M ; appropriate expressions for these quantities are in Appendix A.

Given $\Phi(L|M)$, we compute various “observable” properties of the galaxy population associated with an average dark matter halo of mass M :

- the mean number of galaxies $\langle N \rangle(M)$ (see equation B1);
- the luminosities of the central galaxy L_{cen} and satellite galaxies L_{sat} (see equation B3);
- the morphological type of each galaxy (i.e. early- versus late- type; see appendix B).

All of these properties can be recovered using analytic dark matter halo mass functions, but a cosmological N -body simulation is required to assign phase space coordinates to mock galaxies. In what follows, we describe briefly the main steps involved in constructing the mock catalogues. A more detailed description is provided in appendix B.

2.3.2 Populating Dark Matter Haloes with Galaxies

We perform a series of cosmological N -body simulations following the formation of structure in a ΛCDM model from $z=50$ to $z=0$. Each simulation contains 256^3 particles. We adopt cosmological parameters of $\Omega_m=0.3$, $\Omega_{\Lambda}=0.7$ and $h=0.7$, and the power spectrum of initial density perturbations (generated using CMBFAST Seljak & Zaldarriaga 1996) is normalised assuming a mass variance of $\sigma_8=0.9$. Details of the runs are presented in Table 2. We quote results using the five $100 h^{-1} \text{ Mpc}$ boxes (labelled “A” through “E”), but have verified using the smaller boxes that this resolution is sufficient to reproduce the statistical properties of the mock catalogues.

These simulations provide the dark matter host haloes that we populate with mock galaxies. Haloes are identified at $z=0$ using the friends-of-friends (FOF) algorithm with a linking length of $b=0.2$ times the mean interparticle separation. For each halo we compute its virial mass and radius, and we record also the coordinates of its most bound particle and a list of all particles that reside within its virial radius. This is (in principle) all the information we need to

construct our mock galaxy catalogues.

We note that $\tilde{\Phi}^*$, \tilde{L}^* , and $\tilde{\alpha}$ are functions of halo mass M , but they also depend on the cosmological parameters. Yang et al. (2003) presented a number of different CLFs for different cosmologies and different assumptions regarding the free parameters, and we adopt those used by Y04, who assumed a flat Λ CDM cosmology with $\Omega_m=0.3$, $\Omega_\Lambda=0.7$, $h=0.7$ and a normalisation $\sigma_8=0.9$. Precise values for the CLF parameters are given in appendix A.

These parameters were chosen to recover the observed luminosity functions and correlation lengths of galaxies in the 2dFGRS (both as a function of their luminosity and their type), but we find that the clustering and luminosity functions of galaxies in our mock catalogues are in very good agreement with the corresponding SDSS correlation and luminosity functions.

It is important to estimate the minimum reliably resolved halo mass M_{\min} ; below this threshold the number density of haloes tends to be suppressed relative to the number density they would have in the limit of infinite numerical resolution. In this work we assume that the mass function is converged for haloes containing 50 particles or more (see discussion in Appendix B); this gives $M_{\min}=50 m_{\text{part}}$ in Table 2.

Knowing M_{\min} allows us to estimate L_{\min} , the minimum luminosity that we can assign to a mock galaxy, using the “conditional probability distribution” $P(M|L)$. L_{\min} fixes the halo occupation number, the average number of galaxies per halo of mass M , $\langle N \rangle(M)$ (Equation B1); as M_{\min} and therefore L_{\min} increases (decreases), $\langle N \rangle(M)$ increases (decreases). The mass resolution of our simulations means that we adopt $L_{\min} = 1.1 \times 10^9 h^{-2} L_\odot$ in our mock catalogues A to E, upon which our analysis is based.

We assume that the number of galaxies N in a dark matter halo is Poisson distributed about $\langle N \rangle(M)$ (Yang et al. 2003), and that each galaxy is assigned a luminosity drawn from $\Phi(L|M)$. The central galaxy is defined to be the brightest galaxy in the halo and has a luminosity $L > L_1$, where L_1 satisfies the condition that $\langle N \rangle(M) = 1$ (see Equation B3). The remaining $N-1$ galaxies have luminosities that are drawn randomly from the luminosity function in the range $L_{\min} < L < L_1$.

The morphological type of each galaxy is obtained from $f_{\text{late}}(L, M)$ (equation B4), the probability that a galaxy of luminosity L hosted by a dark matter halo of mass M is late-type. Finally, the position and velocity of the central galaxy are associated with those of the most bound particle in the halo, while the positions and velocities of the remaining $N-1$ galaxies are obtained by randomly sampling the particles in the FOF group.

A more detailed description of our approach to populating dark matter haloes with galaxies is given in Appendix B.

2.3.3 Constructing a Mock Galaxy Redshift Survey

At this point we depart from Y04, who wished to study a mock 2dFGRS and stacked simulation boxes to recover the survey’s median redshift. Our needs are more modest – we wish to evaluate the reliability of our sample selection

criteria. To transform our raw mock galaxy distribution into a mock galaxy catalogue,

- We select a single simulation box, recalling that each box has periodic boundary conditions, and we replicate it 3 times along each dimension, producing a stack of $3 \times 3 \times 3$ boxes. We then centre the stacked boxes on the median redshift of the SDSS $z_{\text{med}}=0.11$.
- We place a virtual observer at $z=0$ and we define an (α, δ) coordinate frame with respect to the centre of the stacked box.
- We compute a redshift z for each galaxy as seen by the virtual observer from the recessional velocity $cz = Hr + \vec{v} \cdot \vec{r}/|r|$, where the galaxy is at \vec{r} with respect to the virtual observer, and $\vec{v} \cdot \vec{r}/|r|$ is its line-of-sight velocity. We account for observational velocity uncertainties by adding a random velocity drawn from a Gaussian of width 30 km s^{-1} . We also compute the apparent magnitude according to its luminosity and distance, to which we add an RMS error of 0.02 mag, in accordance with the SDSS internal estimates of the redshift and photometric errors for galaxies.
- We remove the redshifts of all galaxies that fall below the magnitude limit $r = 17.77$ of the SDSS Main galaxy sample and those with declinations less than $+30^\circ$, for which the depth of the stacked simulation boxes is insufficient and which we define as the edge of the mock survey boundary

There are a number of attributes of the observed survey that are not accurately reproduced by the mock survey. The true survey boundary is much more complicated than the boundary of our mock catalogue, and hence a much larger fraction of galaxies lie near an edge and may be near an unseen bright galaxy. Also, the true survey is not spectroscopically complete, and is less complete in regions of higher density due to the lower availability of fibres. Therefore, our analysis using the mock catalogues would underestimate the importance of excluding primaries near the survey edge, excluding primaries near the magnitude limit of the survey, and implementing a cut based on N_{viol} . As these issues cannot be addressed well using the mock catalogues, we do not implement them in our analysis of the mock catalogue. Their effects on the sample are investigated empirically in § 3.1.

2.3.4 Tests of our Selection Criteria

Using the mock catalogues, we quantify the degree to which current and previous selection criteria accurately identify physical satellites of isolated galaxies. We quote the results of the “Mock A” catalogue (see Table D1), but the results are consistent with those from the other mock catalogues.

Interlopers are identified in the mock catalogues as satellites that do not belong to the same halo as their selected primary galaxy.³ We do not consider primary galaxies as isolated if:

- they are not the central galaxy of their halo, or

³ Note that many previous works refer to all unwanted satellites as “interlopers”, regardless of the reason for wanting to exclude them from the sample. We prefer to designate only satellites that are not physically associated with their selected primary as “interlopers” to distinguish them from satellites that are physically associated with unwanted primaries.

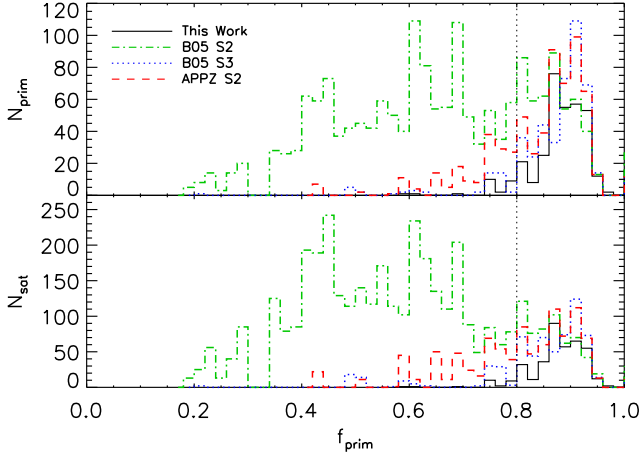


Figure 2. (*Top*) Histogram of the number of primaries selected from the mock catalogue as a function of f_{prim} , the fraction of the true halo luminosity that comes from the primary galaxy. The solid lines represent systems chosen using our adopted selection criteria, while the other line styles indicate other representative criteria (dashed, dotted and dot-dashed for B05 S2, B05 S3 and APPZ S2). (*Bottom*) As above, but weighted per satellite in the sample. The vertical dotted lines denote the f_{prim} below which primaries are considered non-dominant.

(ii) they are not sufficiently more massive than other galaxies within the halo.

Point (i) is easily determined from the mock catalogues because we know which galaxy is the central galaxy of each halo. Point (ii) is more difficult to determine because the CLF formalism assigns luminosities and not masses to individual galaxies. However, we can estimate the degree to which the primary galaxy dominates its halo by calculating the fraction of the total halo luminosity that is contributed by the primary galaxy,

$$f_{\text{prim}} \equiv L_{\text{prim}}/L_{\text{tot}}. \quad (2)$$

In the top panel of Figure 2 we plot a histogram of the number of selected primaries as a function of f_{prim} for four sample sets of criteria (ours, B05 S2, B05 S3 and APPZ S2) that span the range of observed behaviours. In the bottom panel, we weight each primary by its number of selected satellites to demonstrate its influence on the observed sample. Because primaries that contribute less to the luminosity of their halo have more satellites, the tail to low fractions is exacerbated. The histograms are characterised by a symmetric peak centered at $f_{\text{prim}} = 0.9$ that extends down to 0.8 that we identify as truly isolated primaries, and a long tail to low values that we wish to eliminate. Based on examination of these histograms, we consider a primary to be “non-dominant” if $f_{\text{prim}} < 0.8$ (denoted by the vertical line in Figure 2).

Table 3 lists the number of primaries and satellites selected from the mock catalogue that pass and fail the above interloper and isolation criteria. Row 1 indicates the number of primaries selected, row 2 indicates the fraction of those primaries that are not the central galaxy of their halo (category (i) above), row 3 indicates the fraction of primaries that do not dominate the dynamics of their halo (category (ii) above), and row 4 indicates the fraction of selected pri-

maries that are truly isolated. Row 5 indicates the number of satellites selected, row 6 indicates the fraction of those satellites that are “multi-homed”, i.e. selected as satellites of more than one primary, row 7 indicates the fraction of satellites that do not belong to the same halo as their selected primary (“interlopers”), row 8 indicates the fraction of satellites that are physically associated with non-dominant primaries (“ $f_{\text{non-dom}}$ ”), and row 9 indicates the fraction of selected satellites that are selected correctly, i.e. they are physically associated with isolated primaries.

When evaluating criteria based on different bandpasses, we use the following simple transformations: for the AZPK criteria, which are based on RC3 B_T magnitudes, we assume a constant $B - {}^{0.1}r = 0.6$, typical of the late-type galaxies they studied; for the APPZ criteria, we assume a constant difference between the $z = 0$ and $z = 0.1$ r -band k -corrections of 0.23 mag; and for the SL04 criteria, which are based on UK Schmidt b_J magnitudes, we assume a constant $b_J - {}^{0.1}r = 0.7$, intermediate between the typical values for early and late type galaxies.

The use of the mock catalogues to evaluate selection criteria for studies that did not use SDSS data is not as accurate as for those studies based on SDSS because the parameters of the mock catalogues, such as the typical photometric and redshift error, are specifically tuned to mimic SDSS. The photometric errors in ZSFW and the velocity errors in SL04 are significantly larger.

All sets of criteria do an adequate job of selecting central galaxies as primaries and of minimizing the fraction of interlopers and multi-homed satellites, with each source of contamination contributing less than 5% to each sample⁴. However, the fraction of the sample that lies around non-dominant primaries ($f_{\text{non-dom}}$) extends from a low of 6% for our adopted criteria to almost 85% in the case of B05 S2. The greatest single predictor of the magnitude of $f_{\text{non-dom}}$ is whether non-satellites are permitted to lie within the satellite cylinder. In other words, criteria with $m_{\text{sat}} > m_{\text{inner}}$ generally fail to select isolated primaries. Although we do not evaluate the effects of N_{viol} using the mock catalogues, neglecting to account for spectroscopic incompleteness is the other factor that can result in galaxies larger than satellites lying within the satellite cylinder; we therefore expect that this also has a significant effect on $f_{\text{non-dom}}$. The impact of non-dominant primaries on the results will be discussed in detail in § 4.

We have optimized the parameters we use for the selection criteria using the mock catalogues to maximize both the size of the sample (Row 5) and the fraction of the sample that passes all of the checks (Row 9). In particular, all parameters in Table 1 were varied in turn and the new value kept if it increased the sample size without a correspondingly large increase in either the incorrectly-selected fraction (the inverse of the value in Row 9), the interloper fraction, or the fraction of satellites around non-dominant primaries; or, conversely, if it decreased the incorrectly-selected fraction without a correspondingly large decrease in sample size.

⁴ Although it is in principle possible to select multi-homed satellites using many of the sets of criteria, only for B05 S2 does this situation ever occur in practice.

Table 3. Results of Applying Selection Criteria to Mock Catalogues

Parameter	This Work	ZSFW	SL04	S1	B05 S2	S3	AZPK	APPZ S1	S2	AB07
Selected primaries	337	135	1516	1828	1778	404	114	1595	636	589
Non-central primary fraction	0.000	0.007	0.001	0.002	0.002	0.002	0.000	0.003	0.000	0.005
Non-dominant primary fraction	0.071	0.059	0.600	0.640	0.724	0.087	0.123	0.656	0.272	0.626
Isolated primary fraction	0.929	0.941	0.400	0.360	0.276	0.913	0.877	0.344	0.728	0.374
Selected satellites	388	187	2396	3461	3852	563	133	3081	980	1112
Multi-homed fraction	0.000	0.000	0.000	0.000	0.001	0.000	0.000	0.000	0.000	0.000
Interloper fraction	0.046	0.048	0.037	0.036	0.038	0.025	0.023	0.042	0.036	0.049
$f_{\text{non-dom}}$	0.062	0.102	0.691	0.767	0.844	0.151	0.218	0.778	0.409	0.754
Correctly-selected satellite fraction	0.892	0.861	0.290	0.216	0.138	0.824	0.759	0.203	0.563	0.224

When in doubt, we erred on the side of more restrictive criteria. This process was repeated until convergence.

2.4 The Sample

The following quality cuts are imposed on the sample:

(i) Satellites within $35 h^{-1}$ kpc of the primary are removed due to the known sky subtraction problem around bright sources (Mandelbaum et al. 2005, 2006) and the possibility of bright knots in the outer regions of a galaxy being mistakenly deblended as separate galaxies.

(ii) As the interloper fraction rises at large projected radius, and the radius at which interlopers dominate increases with halo mass, we eliminate satellites of less luminous ($M_r - 5 \log h > -21.2$, i.e. fainter than the median) primaries which lie beyond a projected radius of $345 h^{-1}$ kpc; this choice of parameters is justified below.

The resulting sample of primary and satellite galaxies is given in Table 4. The full sample contains 428 satellites of 361 primaries; 260 (101) of the primaries are classified as early-type (late-type) hosting 317 (111) satellites.

The following cuts are further imposed on systems used to measure the anisotropy around primary galaxies:

(i) Primaries that do not have a measured position angle (PA) in the SDSS DR5 database are excluded; this cut excludes 7 primaries.

(ii) Primaries with isophotal axis ratios $b/a > 0.8$ are excluded. Galaxies with nearly circular isophotes have poorly-constrained PAs. In addition, any anisotropy that exists in three dimensions gets washed out in projection as the system is viewed close to its axis of symmetry. The numerical choice of $b/a > 0.8$ for this cutoff is motivated in § 3.1 and the effects of changing this value are discussed.

Unless otherwise specified, this subsample is the sample referred to for the remainder of the paper, and contains 238 satellites of 201 primaries. In § 3.2, we analyze the distribution of satellites with respect to the large scale structure (LSS). For those purposes, the following further cuts are imposed instead:

(i) Systems within a projected radius $3000 h^{-1}$ kpc of the edge of the spectroscopic survey footprint are excluded in order to ensure that the survey boundary does not introduce a bias in the derived LSS axis.

(ii) Primaries for which the LSS axis is undefined because there are no galaxies within the cylinder used to define the axis or for which the LSS axis ratio is greater than 0.9 are excluded.

This subsample contains 281 satellites of 239 primaries.

The distribution of luminosities, number of satellites per primary, radial separations and velocity differences are shown in Figure 3. In Figure 3a we plot the absolute magnitude distributions of the primary and satellite galaxies, along with the magnitude difference. The median absolute magnitude is $M_r - 5 \log h = -21.2$. The typical primary has a luminosity similar to the Milky Way, while the typical satellite is ~ 2.5 magnitudes fainter, slightly brighter than the LMC. Figure 3b shows the number of satellites per primary. Most primaries are surrounded by only one satellite. Figure 3c presents the distribution of radial separation between satellites and primary galaxies for samples split by the type and luminosity of the primary (the median absolute magnitude, -21.2 is used as the cutoff between the “bright” and “faint” subsamples). In this panel only, we include the distant satellites of faint primaries. The radial distribution of true satellites declines with radius, while the distribution of interlopers increases with radius (Chen et al. 2006). The crossover between these regimes occurs at the edge of the dark matter halo, and therefore depends on galaxy mass. Figure 3d shows no evidence for an increase in the number of outer satellites due to interlopers around bright primaries. However, such an upturn is evident around faint primaries of both morphologies beyond $\Delta R > 345 h^{-1}$ kpc. Therefore, around primaries with $M_r - 5 \log h > -21.2$ we exclude satellites at projected radii $\Delta R > 345 h^{-1}$ kpc in all other panels and remaining plots. Figure 3e presents the distribution of velocity differences between satellites and their primaries. The velocities of selected satellites cluster strongly about the velocity of the primary indicating that they are indeed physically associated. The velocity dispersion of satellites around bright primaries is higher than around faint primaries due to their larger mass (see, e.g. Norberg et al. 2007; Conroy et al. 2007, and references therein).

Landscape table to go here.

Table 4.

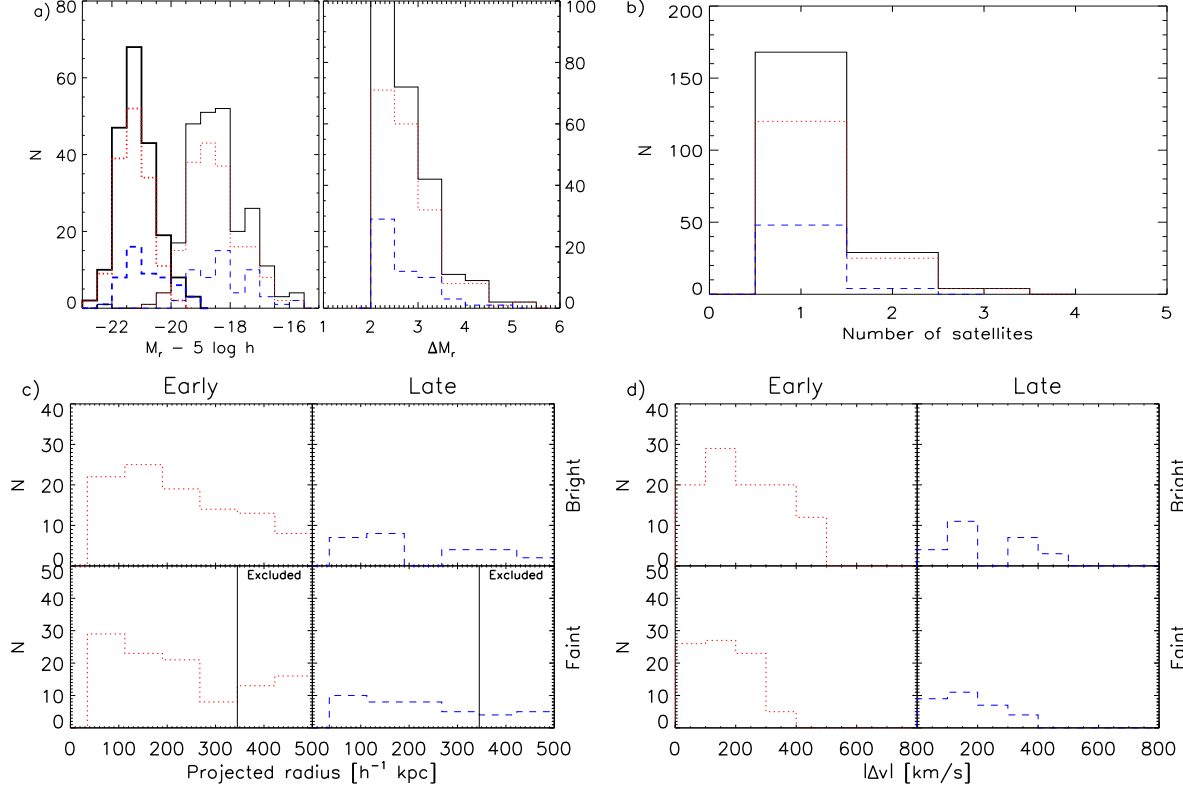


Figure 3. (a) Absolute magnitude distributions of primary galaxies (thick lines) and of satellites (thin lines) (left panel) and the difference between the magnitude of each satellite and its primary (right panel). The red/dotted lines shows the distribution for early-type primaries while blue/dashed lines refer to late-type primaries. Note that the satellites are also separated according to the type of their primary, not according to their own type. (b) Distribution of number of satellites per primary. Line colours/styles indicate the classification of the primary galaxy as in (a). (c) Distribution of projected radial separation of satellites from their primary. Left panels show satellites of early-type galaxies while right panels show satellites of late-type galaxies. Top panels show satellites of primary galaxies more luminous than the median ($M_r - 5 \log h < -21.2$) while bottom panels show satellites of the less-luminous primary galaxies ($M_r - 5 \log h > -21.2$). The vertical lines mark the maximum radial extent for satellites of faint primaries. These satellites are not included in the remaining plots. (d) Distribution of velocity differences between satellites and their primary. Panels are as in (c).

3 RESULTS

3.1 Distribution About The Primary Galaxy: The Holmberg Effect

We define the “disc angle” as the angle between the r -band isophotal position angle of the major axis of the primary and the PA of the great circle between the primary and satellite (see Figure 1); we fold this angle into the range $0-90^\circ$. If satellites are distributed isotropically around the primaries then the distribution of disc angles is uniform with a mean of 45° .

In Figure 4 we plot the cumulative and differential disc angle distributions. The full sample shows a tendency to lie at small disc angles, i.e. for the satellites to lie near the major axis of their parent galaxy. The hypothesis that the angles are distributed randomly is ruled out with high significance: according to the Kolmogorov-Smirnov (KS) test, the probability is 0.03 with a mean disc angle of $41.4^{+1.7}_{-1.6}$.

The individual distributions of satellites around early-type and late-type primaries are much more extremely anisotropic, but in opposite senses: the excess concentration of satellites is along the major axis for early-types but along the minor axis for late-types. The mean disc angles

are $38.9^{+1.7}_{-1.9}$ and $50.6^{+3.7}_{-3.6}$, with KS test probabilities of being drawn from a random distribution of 3×10^{-4} and 0.14 for satellites of early-type and late-type primaries respectively. When the samples are combined these effects counteract each other, reducing the measured anisotropy around the full sample, which contains more satellites of early-type galaxies than late-type galaxies and therefore shows a major-axis alignment. The KS test results, the mean and median disc angles, and the polar fraction (the fraction of satellites with disc angles larger than 45°) are listed in Table 5. The quoted uncertainties are determined using bootstrap resampling of the primaries and represent 68% confidence intervals. All statistics reinforce the same conclusion: satellites of disc galaxies lie along the pole (The Holmberg Effect) while satellites of early-types tend to lie near the long axis of the spheroid. We have verified using the mock catalogues, which have intrinsically isotropically-distributed satellites, that we could not have measured such a strong anisotropy around either the early or late-type primaries if it were not physically present; see Appendix D.

Our measured alignment must be a lower limit on the intrinsic three-dimensional alignment for several reasons. Firstly, images of triaxial elliptical galaxies contain isopho-

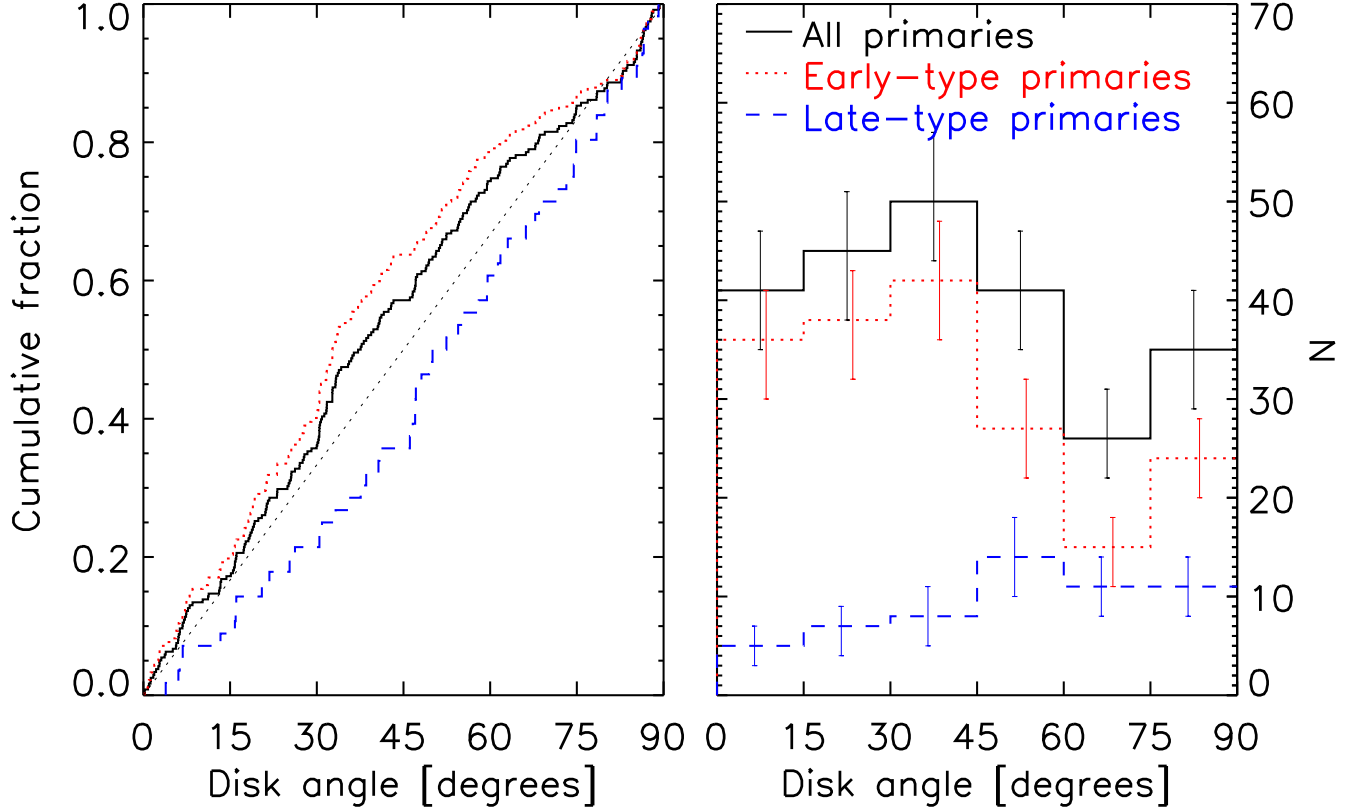


Figure 4. (Left) Cumulative distribution of angle between the major axis of the primary and the location of the satellite (“disc angle”). The thick black/solid, red/dotted, and blue/dashed lines refer to the distribution of satellites around all primaries, early-type primaries, and late-type primaries respectively. The thin dotted line shows the distribution expected if satellites were isotropically distributed. (Right) Differential distribution of the disc angles. The error bars are determined by bootstrap resampling of all primary galaxies.

Table 5. Anisotropy of Satellite and Primary Distributions

Parameter	Full sample	Early-type primaries	Late-type primaries
Disc angle:			
KS probability	0.03	0.0003	0.14
Mean disc angle [°]	$41.4^{+1.7}_{-1.6}$	$38.9^{+1.7}_{-1.9}$	$50.6^{+3.7}_{-3.6}$
Median disc angle [°]	$37.6^{+2.9}_{-3.4}$	$33.2^{+1.5}_{-2.4}$	$50.0^{+8.0}_{-2.9}$
Polar fraction	0.43 ± 0.03	0.37 ± 0.03	$0.65^{+0.08}_{-0.07}$
Early-type satellite mean	40.0 ± 2.9	$38.7^{+3.1}_{-3.4}$	$56.0^{+8.2}_{-7.5}$
Late-type satellite mean	$42.1^{+1.9}_{-2.1}$	$39.0^{+2.5}_{-2.2}$	$49.9^{+4.1}_{-3.5}$
LSS angle:			
KS probability	0.18	0.38	0.76
Mean LSS angle [°]	43.2 ± 1.6	43.1 ± 1.9	$43.4^{+3.1}_{-3.5}$
Mean disc/LSS angle:			
Primaries with satellites	$41.4^{+1.9}_{-1.8}$	40.2 ± 2.2	45.3 ± 4.2
All isolated primaries	42.9 ± 1.0	41.8 ± 1.2	$45.3^{+1.8}_{-1.9}$

tal twists due to projection effects, which introduces scatter between the isophotal PA we use and the intrinsic 3D major axis. Secondly, galaxies seen closer to their symmetry axis have their anisotropic signal diluted. Finally, interlopers will dilute the signal.

In Figure 5a, we plot the mean disc angle of satellites as a function of projected separation from their primary. Satellites are binned in 3 annuli spaced evenly in radius from $35 h^{-1}$ kpc to $500 h^{-1}$ kpc, and are separated into those more luminous and less luminous than the median

$M_r - 5 \log h = -21.2$. The anisotropy appears to increase with distance from the primary around early-type galaxies, suggesting that the anisotropy is driven externally. On the other hand, the anisotropy around late-type galaxies peaks at intermediate separations; the interpretation for this is not clear. This intermediate bin covers approximately the same radii as the outermost bin of AB07, in which they also detect minor-axis alignment. While we do not detect the major-axis alignment that they see at small radii, a large number of systems in their innermost radial bin fall within the $35 h^{-1}$ kpc

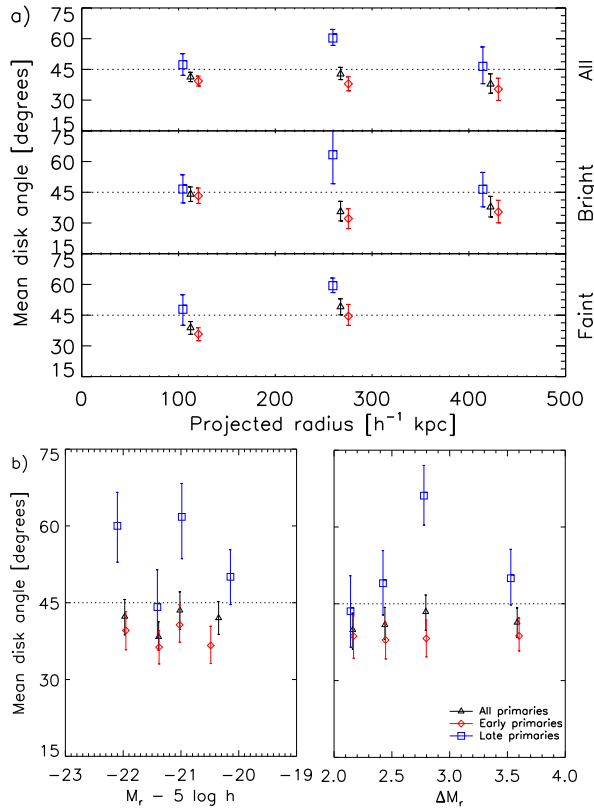


Figure 5. (a) Mean disc angle of satellites as a function of projected separation from their primary. Black/triangles, red/diamonds, and blue/squares refer to satellites of all primaries, early-type primaries, and late-type primaries respectively. Radial bins are $155 h^{-1}$ kpc wide and are plotted at the central bin radius, with diamonds and squares offset for clarity. The top panel contains all satellites while the middle and bottom panels contain satellites of primaries with $M_r - 5 \log h < -21.2$ and $M_r - 5 \log h > -21.2$ respectively. (b) Mean disc angle of satellites as a function of the absolute magnitude of the primary (left) and magnitude difference between the primary and satellite (right). Bins are chosen to have approximately equal number of satellites per bin and are plotted at the mean magnitude.

region that we exclude to avoid contamination from H II regions in the outskirts of the parent galaxy; if such regions are mistakenly included as satellites, they will bias the result towards major-axis alignment.

In Figure 5b, we compare the anisotropy as a function of the luminosity of the primary, and of the difference in magnitude between the primary and satellite. In the left panel, the galaxies are placed in bins 1 magnitude wide, while in the right panel the widths of the bins are chosen such that there are similar numbers of satellites in each bin; in both panels, the symbols are plotted at the mean luminosity or ΔM_r of the galaxies in the bin. No clear trend is apparent as a function of luminosity, while there is a slight tendency for the fainter satellites of late-type galaxies to show a stronger anisotropy than the brightest satellites.

Koch & Grebel (2006) found that the early-type satellites of M31 have a more polar alignment than the late-type satellites. Y06 and Faltenbacher et al. (2007) found that the red satellites of red primaries show stronger major-axis alignment than the blue satellites. To determine if either

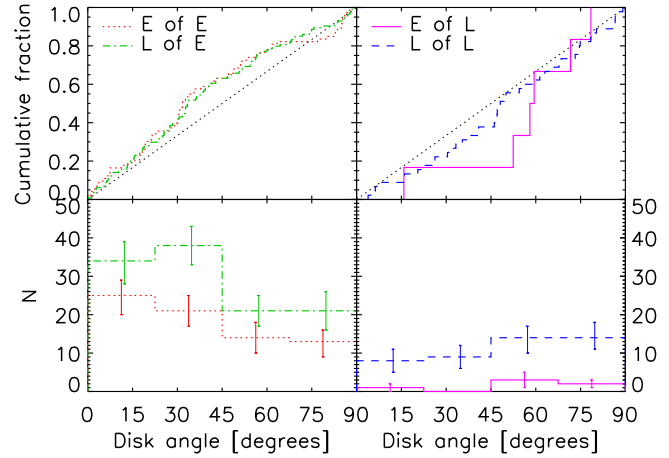


Figure 6. Cumulative (top) and differential (bottom) distributions of disc angle as a function of morphological type of both the primary and satellite. Red/dotted (green/dot-dashed) lines denote early- (late-) type satellites of early-type primaries, while blue/dashed (magenta/solid) lines denote early- (late-) type satellites of late-type primaries.

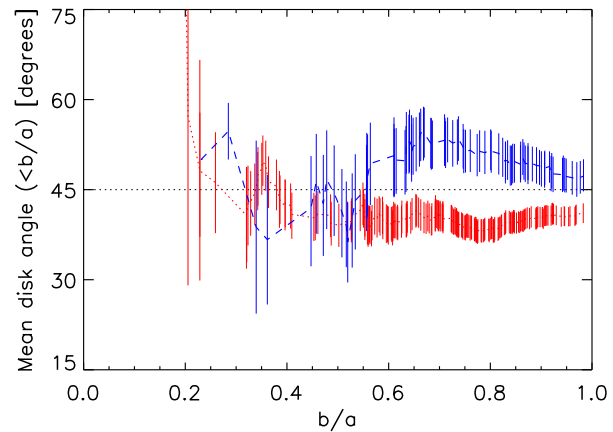


Figure 7. Mean disc angle for satellites of primaries with isophotal axis ratios less than or equal to the plotted abscissa. One error bar is plotted at the location of each primary galaxy. Colors/line styles are as in Figure 5.

signal is evident in our sample, we split the sample by the galaxy type of both the primary and satellite and plot the distributions in Figure 6. Mean disc angles for early- and late-type satellites are given in Rows 5 and 6 of Table 5. We do not detect any difference between the alignment properties as a function of the satellite type; the anisotropy is dominated by the type of the primary.

In § 2.4, we excluded primary galaxies with isophotal axis ratios $b/a > 0.8$. Our choice of cutoff is motivated by Figure 7, where we plot the mean disc angle around primaries with axis ratios less than or equal to the plotted abscissa. Including galaxies with $b/a > 0.8$ dilutes the signal, both for early- and late-types. For a circular disc galaxy of intrinsic thickness 0.2, this corresponds to an inclination of 43° . The strength of the decline in anisotropy with axis ratio is not as strong for early-type galaxies as for late-types. We suspect that this is because early-type galaxies tend toward prolateness (Vincent & Ryden 2005),

and therefore the three-dimensional major axis maintains its uniqueness in projection even for apparent axis ratios approaching unity. The decline in anisotropy around late-types may also be exacerbated by non-axisymmetric structures such as spiral arms, dust lanes and intrinsic ellipticity (Simon et al. 2005) that affect the isophotes of late-type galaxies when seen nearly face-on but do not affect early-types.

As discussed in § 2.3.3, it is difficult to assess the effects of some of the selection parameters using the mock catalogues. Therefore, we now empirically investigate the effects of varying all of the selection parameters, including several parameters that have been neglected by many previous studies. In Figure 8, we plot the mean disc angle and the sample size as we adjust N_{viol} , f_{sat} , and whether or not the survey magnitude limit or survey edge are taken into account. The mean disc angle for early and late-type galaxies are shown as symbols with error bars while the sample sizes are shown as histograms above and below.

In panel (a), we plot both our photometric redshift-based method of dealing with potential violators and those based on a cut on N_{viol} . More restrictive values of N_{viol} lead to smaller sample sizes, particularly for $N_{\text{viol}} \leq 4$. However, the measured anisotropy around both early- and late-type primaries increases as the sample becomes more restrictive, indicating that the distribution around truly isolated galaxies is very anisotropic, but samples using larger values of N_{viol} or which do not take into account the presence of non-spectroscopic galaxies at all are significantly contaminated, reducing the measured anisotropy. Our photometric redshift method produces a sample size equivalent to using $N_{\text{viol}} = 1$, but with a measured anisotropy more similar to that found using $N_{\text{viol}} = 0$, indicating that it efficiently separates true neighbours from apparent neighbours. In panel (b), we plot the effects of f_{sat} . The measured anisotropy around early-type galaxies shows a steady increase as f_{sat} is reduced below 0.25; this is accompanied by a steady decrease in sample size that is particularly pronounced below 0.15. The measured anisotropy around late-type galaxies shows a dramatic increase for $f_{\text{sat}} \leq 0.1$ concurrent with a dramatic decrease in sample size. This indicates that the anisotropy is directly related to the dominance of the primary galaxy, and samples selected with values of $f_{\text{sat}} > 0.2$ are significantly contaminated. In panel (c), we show the effects of ignoring the survey magnitude limit or of ignoring the survey edge. Ignoring the magnitude limit increases the sample size slightly without affecting the results. This is because the existence of a satellite galaxy around a primary already requires that the primary be almost as bright as the limit imposed by the survey magnitude limit cut, and therefore any unseen criteria-violating neighbour can only violate the criteria by a marginal amount. On the other hand, ignoring the edge of the survey increases the sample by a slightly larger amount but reduces the measured anisotropy around late-type galaxies significantly. This is because we have no knowledge about the missing neighbourhood around any galaxy near the survey edge; given the small fraction of galaxies that satisfy our strict isolation criteria when their full environment is known, a large fraction of the galaxies close to the survey edge are likely to not be isolated.

The quantitative measurement of anisotropy is dependent on these often-neglected selection parameters, espe-

cially f_{sat} and N_{viol} ; however, the qualitative result, that the satellites of disc galaxies show a polar distribution while the satellites of spheroidal galaxies show a major-axis distribution, is not dependent on the value of any one of these parameters. Although the influence of each of these parameters on the sample is entirely independent (based on the presence of nearby non-spectroscopic galaxies for N_{viol} , the ratio of satellite to primary luminosity for f_{sat} , and the proximity to the survey edge and apparent magnitude in the case of panel (c)), in every case galaxies selected using more restrictive isolation criteria exhibit *more* anisotropic satellite distributions. This provides strong evidence that the anisotropy is physical. Varying the other parameters from Table 1 has very little effect on the measured anisotropy, as anticipated by the results of B05, who found identical results in three samples with quite different values of these parameters.

3.2 Satellite and Primary Distribution Relative to Large Scale Structure

If satellites are accreted from filaments, then the most recently-accreted satellites will be aligned preferentially with the surrounding filamentary large scale structure (LSS). We test this expectation by determining the axis of the LSS surrounding each primary galaxy. To determine this axis, we use all spectroscopic galaxies with projected radii between 1000 and 3000 h^{-1} kpc (thereby explicitly ensuring that there is no overlap between the galaxies used to determine the orientation of the LSS and those used to evaluate the isolatedness of the primary or the satellites themselves) with velocities that differ from that of the primary by no more than 400 km s^{-1} . The velocity dimension of this cylinder is significantly smaller than the cylinder used to select isolated galaxies and satellites. This is because filaments are not virialised structures and their intrinsic velocity dispersion about the Hubble flow is much lower than that inside a halo (for example, the scatter about the Hubble flow among the galaxies surrounding the Local Group is a mere 85 km s^{-1} , or as low as 40 km s^{-1} if galaxies inside virialised groups are excluded; Karachentsev et al. 2003), and therefore a much smaller additional velocity is required to account for peculiar velocities on top of the Hubble component of 300 km s^{-1} corresponding to the radial dimension of the cylinder. We calculate the PA and axial ratio of the distribution on the sky of these surrounding galaxies by diagonalising the moment of inertia tensor relative to the primary galaxy. We have used the mock catalogues to confirm that this procedure reliably recovers the three-dimensional PA of the LSS surrounding the primary (see Appendix E).

Figure 9 shows the distribution of angles between the PA of the great circle connecting the primary and the satellite and the PA of the LSS surrounding the primary (“LSS angles”; as with the disc angles, these are folded into the range 0–90°). We present the results from KS tests and the mean LSS angles in Table 5.

The satellites of all galaxies, and of the early- and late-type subpopulations are each consistent with being isotropically distributed with respect to the LSS. However, all samples have mean LSS angles less than 45°. Further data are required to determine if this hint of an alignment is real. In Figure 10, we plot the mean LSS angle as a function of radial separation from the primary. Although each individual point

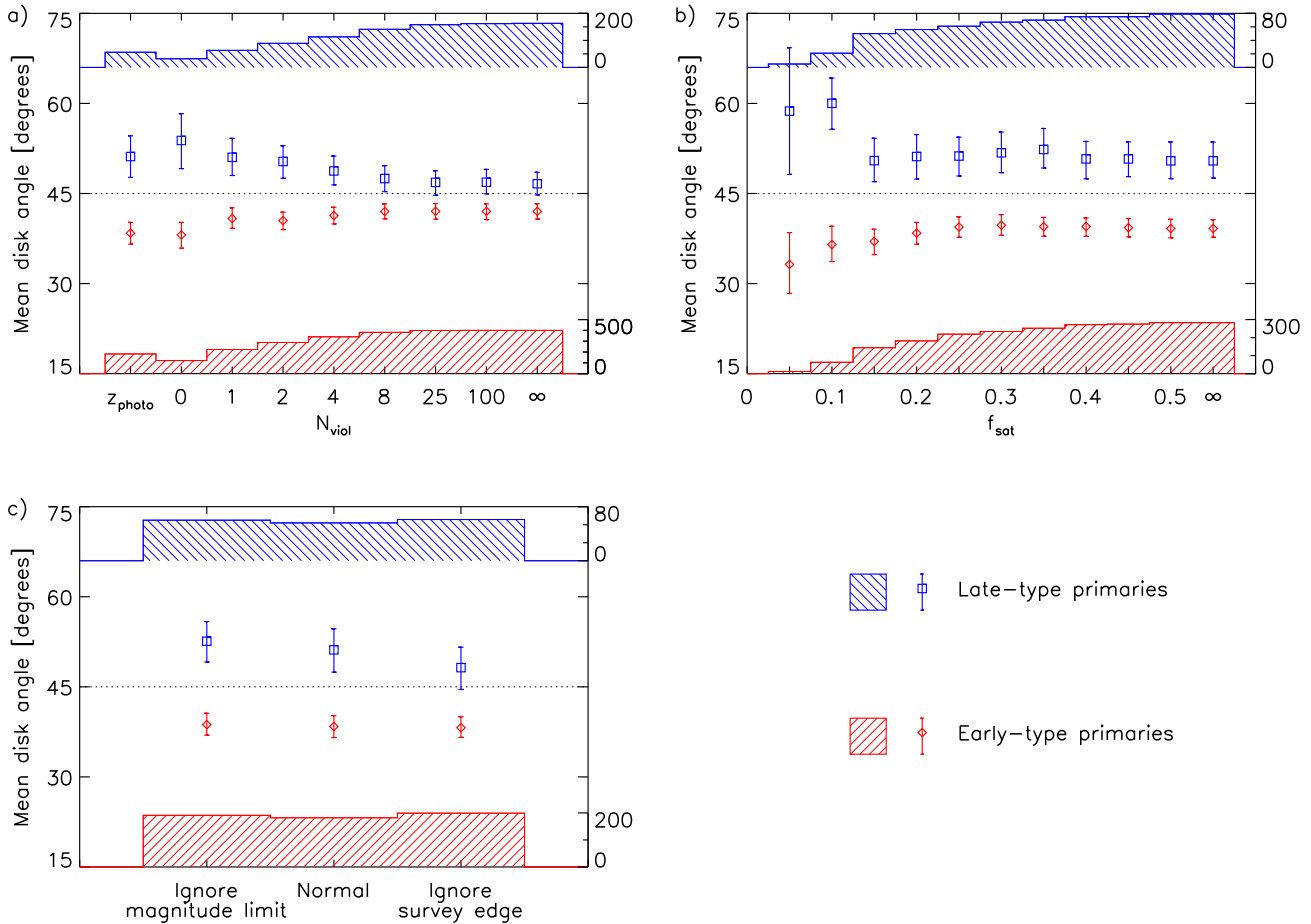


Figure 8. Effects of varying the selection parameters on the results and sample size. In each plot, the mean disk angle for late-type (early-type) primaries is shown as the blue/diamond (red/square) symbols with error bars, while the sample size is shown as the histogram above (below). The shape for each histogram is shown on the right side of each plot. (a) The effects of replacing the fiducial photometric redshift method for dealing with potential isolation criteria violators with a cut on N_{viol} . (b) The effects of changing f_{sat} . (c) The effects of limiting primaries to be at least m_{inner} magnitudes brighter than the survey limit and of limiting primaries to be at least projected radii R_{outer} from the edge of the photometric survey footprint and R_{sat} from the edge of the spectroscopic survey footprint.

is consistent with isotropy, all subsamples around early-type galaxies and all but the nearest subsamples around late-type galaxies individually have mean LSS angles less than 45° . This suggests that the signal is real, and is stronger at larger radii around late-type galaxies.

Given the orientation of the primary galaxy and the LSS, we now investigate their relative alignment. The orientation of a disc galaxy is determined by its angular momentum, which originates from tidal torques due to the surrounding material. Analytic arguments and cosmological simulations suggest that this angular momentum (and therefore the disc spin axis) aligns with the intermediate axis of the surrounding mass distribution, and such alignment has been measured for disc galaxies in the supergalactic plane (Navarro et al. 2004) and for galaxies in SDSS and 2dFGRS on the surfaces of voids (Trujillo et al. 2006). The orientation of an early-type galaxy is determined by its anisotropic velocity ellipsoid, as is that of its halo; therefore, the two are expected to be aligned, and preferentially aligned with the large scale structure (Bailin & Steinmetz 2005). This has been measured for Brightest Cluster Galaxies (BCGs) at low (Argyres et al. 1986; Lambas et al. 1988; Muriel & Lambas

1989) and high (Donoso et al. 2006) redshift, but not for field early-types. We directly compared the PA of our primary galaxies to that of their local LSS. For this comparison, we use all isolated galaxies that pass both the “Disc” and “LSS” quality cuts, regardless of whether they host satellite galaxies; our results are unchanged if we only include those that host satellite galaxies. The distributions are shown in Figure 11, and the associated mean angles are given in Table 5. There is a clear detection of alignment between the orientation of isolated early-type galaxies and the surrounding LSS, while late-type galaxies appear to be oriented isotropically. The samples containing all isolated galaxies and only those with satellites are consistent with each other.

3.3 Satellites in the Local Group

The satellites of the two dominant galaxies in the Local Group, the Milky Way and M31, appear to lie on planes nearly perpendicular to their parent discs (Metz et al. 2007, and references therein). In order to determine how the anisotropy of the SDSS galaxies compares to the anisotropy around the Local Group spirals, we have determined the sig-

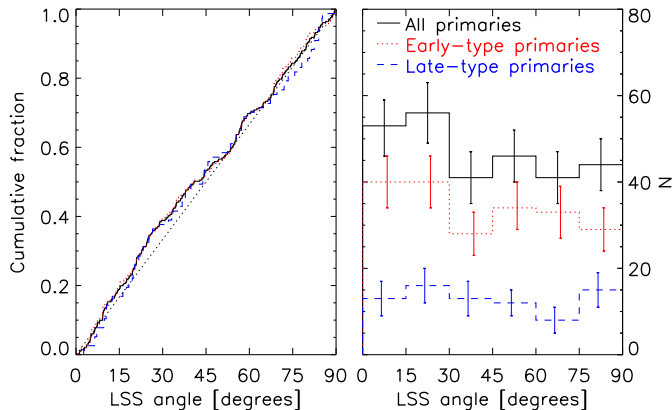


Figure 9. (Left) Cumulative distribution of angle between the axis of the local LSS and the location of the satellite (“LSS angle”). The thick black/solid, red/dotted, and blue/dashed lines refer to the distribution of satellites around all primaries, early-type primaries, and late-type primaries respectively. The thin dotted line shows the distribution expected if satellites are isotropically distributed. (Right) Differential distribution of the LSS angles. The error bars are determined by bootstrap resampling of all primary galaxies.

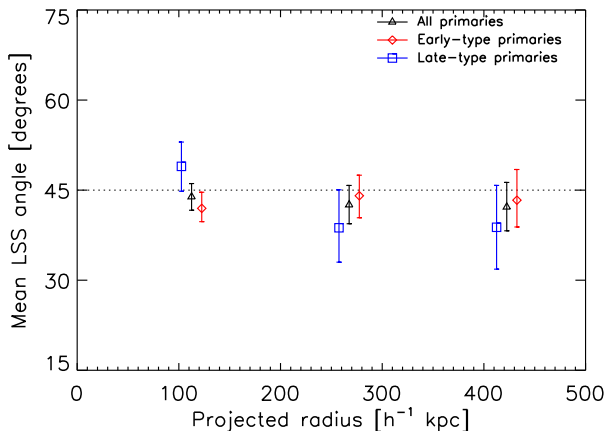


Figure 10. Mean LSS angle of satellites as a function of their projected separation from the primary. Black/crosses, red/diamonds, and blue/squares refer to satellites of all primaries, early-type primaries, and late-type primaries respectively. The diamonds and squares are offset slightly for clarity.

nal we would have recovered around both the Milky Way and M31 if they had fallen into our sample⁵. Based on the distribution of primary and satellite magnitudes in our sample (Figure 3a), we use all satellites with absolute magnitudes within 5 magnitudes of their primary; for the Milky Way this consists of the LMC and SMC, and for M31 this consists of M33, IC 10, M32, and NGC 205. The 3D locations of these satellites with respect to their parent galactic disc are taken from Metz et al. (2007), using the McConnachie & Irwin

⁵ In fact, neither the Milky Way nor M31 would fall into our sample if they were observed in a redshift survey because the presence of each would violate the isolation criteria around the other. Our isolation criteria are required to be so strict in order that systems intrinsically less isolated than Local Group galaxies are not mistakenly included.

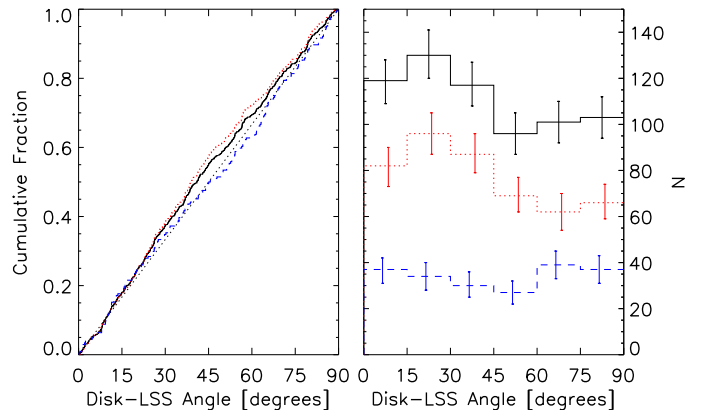


Figure 11. Cumulative (left) and differential (right) distributions of angles between the major axes of isolated galaxies and their surrounding LSS. The sample contains all isolated galaxies that pass the “Disc” and “LSS” sample quality cuts, regardless of whether they host any satellite galaxies. Red/dotted lines refer to early-type galaxies while blue/dashed lines refer to late-type galaxies.

Table 6. Anisotropy of Local Group Satellites

Parameter	Milky Way	M31
Mean disc angle [°]	49.1	54.0
Median disc angle [°]	47.7	53.4
Polar fraction	0.57	0.60

(2006) parameters for the M31 satellites. We select 20000 random viewing directions isotropically distributed about each galaxy and calculate the disc angle for each satellite from each viewing direction. We calculate the mean disc angle of the satellites averaged over all viewing angles where the projected axis ratio of the parent disc is less than 0.8, to provide a direct comparison to the SDSS sample.

The resulting anisotropies are listed in Table 6. The satellites of the Local Group spirals show the same polar distribution with the same magnitude as do the satellites of isolated late-type galaxies in our SDSS sample, with mean disc angles of 49.1° and 54.0° for the satellites of the Milky Way and M31 respectively. This strongly indicates that their satellite distributions are absolutely typical of those around isolated disc galaxies and not simply a coincidence of small number statistics.

4 COMPARISON WITH PREVIOUS RESULTS: THE EFFECTS OF ENVIRONMENT

Our results indicate that the satellites of isolated disc galaxies exhibit a strong preference for lying near the pole of the disc, while the satellites of isolated early-type galaxies show a strong preference for lying near the major axis of the primary. The result of combining these populations gives a distribution that is purely a function of the morphological mixture in the sample of isolated galaxies. Because of the typical luminosities of our primaries, our sample contains more early-types than late-types and therefore we find that satellites tend to exhibit a net major axis alignment.

Table 7. Disc angles compared to previous work

Study	Literature mean [$^{\circ}$]	Our mean [$^{\circ}$]
ZSFW - All	...	$42.6^{+1.4}_{-1.3}$
ZSFW - Early	...	41.6 ± 1.5
ZSFW - Late	48.1 ± 2.6	$47.4^{+3.4}_{-3.0}$
SL04 - All	41.6 ± 1.1 ^a	42.7 ± 0.5
SL04 - Early (P3)	39.8 ± 0.9 ^a	42.3 ± 0.6
SL04 - Late (P4)	44.1 ± 1.7 ^a	$44.2^{+1.2}_{-1.1}$
B05 S1 - All	42.1 ± 0.5	42.2 ± 0.7
B05 S1 - Early	...	41.6 ± 0.8
B05 S1 - Late	...	$44.1^{+1.5}_{-1.6}$
B05 S2 - All	42.1 ± 0.6	41.5 ± 0.5
B05 S2 - Early	...	41.0 ± 0.6
B05 S2 - Late	...	$45.7^{+1.6}_{-1.5}$
B05 S3 - All	42.1 ± 0.9	42.2 ± 0.7
B05 S3 - Early	...	41.6 ± 0.8
B05 S3 - Late	...	44.1 ± 1.6
AZPK - All	...	$44.6^{+1.3}_{-1.5}$
AZPK - Early	...	44.1 ± 1.8
AZPK - Late	44.8 ± 1.9 ^b	47.7 ± 2.4
APPZ S1 - All	...	$42.0^{+0.5}_{-0.6}$
APPZ S1 - Early	43.8 ± 0.5 ^c	41.5 ± 0.5
APPZ S1 - Late	$45.1^{+0.9}_{-1.0}$ ^c	45.1 ± 1.2
APPZ S2 - All	...	$42.0^{+0.7}_{-0.8}$
APPZ S2 - Early	$44.1^{+0.8}_{-0.9}$ ^c	41.3 ± 0.9
APPZ S2 - Late	$45.6^{+1.4}_{-1.3}$ ^c	$44.4^{+1.6}_{-1.7}$
AB07 - All	42.8 ± 0.4	$42.3^{+0.5}_{-0.4}$
AB07 - Early	42.1 ± 0.4	41.9 ± 0.5
AB07 - Late	44.8 ± 0.7	$44.8^{+1.0}_{-0.9}$

^aCalculated from the quoted values of A as described in the text.

^bError calculated as σ/\sqrt{N} assuming Poisson statistics.

^cMean and error calculated from the histogram given in APPZ assuming all satellites lie at the central value of their bin. Error calculated using bootstrap resampling.

Our results for late-type galaxies agree strongly with both Holmberg (1969) and ZSFW, who found a polar alignment. They are in sharp contrast with SL04, AZPK, APPZ, and Y06, who found isotropic distributions around late-types; they contrast with AB07, who detect an isotropic distribution around late-types, although both our study and theirs detect a polar alignment for satellites at projected separations of $\approx 250 h^{-1}$ kpc. Our results for early-type galaxies are in agreement with SL04, Y06, APPZ and AB07, who also found a major-axis alignment. Finally, our results for the full sample agree with SL04, B05, Y06 and AB07, who all found that the full sample shows major-axis alignment.

To determine the effects of the different adopted criteria on the measured anisotropy, we adopt the criteria from the previous studies (as given in Table 1) to select corresponding samples of galaxies from SDSS DR5 and to measure the disc angle distribution. The mean value of the disc angle determined by the previous studies and the value we derive using identical selection criteria are summarised in Table 7 and shown in Figure 12. SL04 do not quote a mean disc angle; rather, they fit the distribution of disc angles θ to the form

$$f(\theta) = A \cos(2\theta) + B \quad (3)$$

and quote the values of A and errors σ_A . To enable a more

direct comparison with other studies, we calculate the mean disc angle of the associated distribution as

$$\langle \theta \rangle = \frac{\pi}{4} - \frac{A}{2} \quad (4)$$

with uncertainty

$$\sigma_{\langle \theta \rangle} = \frac{\sigma_A}{2}, \quad (5)$$

in radians. APPZ also do not quote a mean disc angle. We have derived the mean and the error of the distributions from their plotted histograms, assuming that all satellites lie at the central value of the bin they fall in. The errors are calculated by bootstrap resampling. ZSFW do not quote a mean disc angle, but it can be derived from the data in Table 2 of Zaritsky et al. (1997a). The errors are calculated by bootstrap resampling. We split each sample by the galaxy type of its primary although ZSFW and AZPK only studied late-types, and B05 did not separate the sample by type. B05 suggested that her samples were dominated by systems with late-type primaries; in contrast, we classify 75%/83%/72% of the primaries we select using her criteria as early types, containing 81%/89%/76% of the satellites for samples 1, 2, and 3 respectively (note, however, that Herbert-Fort et al., in preparation, classify several of our early-type systems by eye as discs). The results of Appendix C indicate that different methods of classifying galaxies may introduce $\sim 1\sigma$ differences in the measured anisotropy.

Direct comparison reveals that when we implement the selection criteria of each previous study, we reproduce their results. We recover a polar distribution of satellites around disc galaxies selected as in ZSFW; an isotropic distribution of satellites around late-type galaxies selected as in SL04, AZPK, APPZ or AB07; a major-axis alignment of satellites around early-types selected as in SL04, APPZ or AB07; and a major-axis alignment of the full sample selected as in SL04, B05 or AB07. The only cases where our results deviate from the previous results by more than 2σ are the early-type samples of SL04 and APPZ. Even in these cases, the sense of the observed anisotropy is the same, only the magnitude is different. These are cases where there is no mean disc angle quoted by the authors, and therefore we have used indirect methods to determine the appropriate mean; they also use different methods to classify early-type galaxies. We conclude that the numerical differences in these cases are not significant. Our ability to reproduce the previous results simply by varying the selection criteria confirms that the difference between our conclusions and those of the previous studies are not due to statistical fluctuations or trivial errors in application, but rather to systematic errors caused by sample selection. Furthermore, the distribution of satellites around early and late-type galaxies differs in all samples, and therefore the results obtained for the full sample in any of these studies reflects in large part the relative numbers of early vs. late type primaries in that sample.

Our selection criteria have been fine-tuned using mock catalogues to select satellites of isolated primaries. While most previous authors have also implemented selection criteria aimed at identifying isolated primaries, the results of § 2.3 indicate that they have had variable success. In partic-

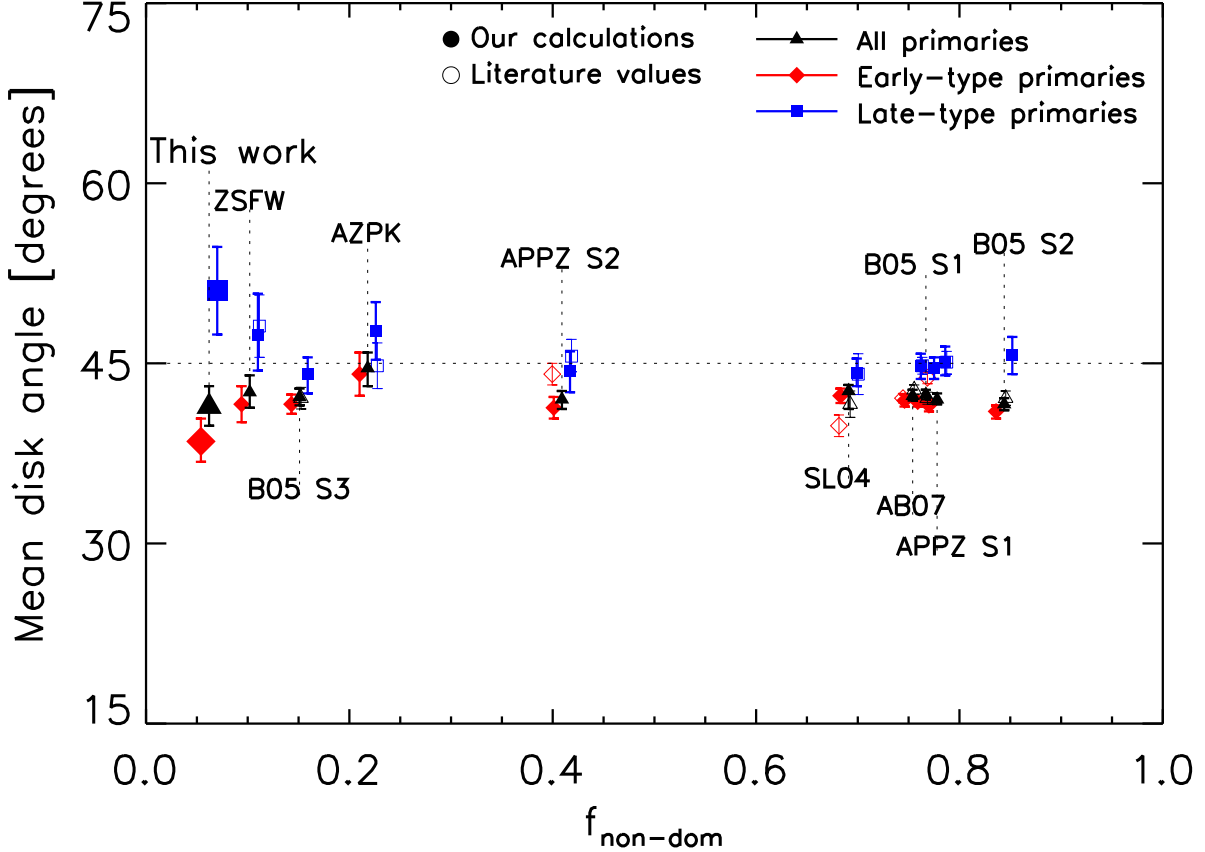


Figure 12. Mean disc angle of satellites selected using each set of criteria vs. $f_{\text{non-dom}}$, the fraction of satellites selected using each criteria that lie around non-isolated primaries (see Table 3). Colors/symbols are as in Figure 5. Filled symbols with thick error bars indicate our calculations, while open symbols with thin error bars indicate the values given in each previous study. As the degree of agreement is excellent, the filled and open symbols typically lie almost on top of each other. Early and late-types are offset for clarity.

ular, the fraction of satellites around non-isolated primaries is over 50% in several of the previous studies. The satellites in these systems should be considered group members rather than satellites of isolated galaxies. The criteria of Y06 and Faltenbacher et al. (2007) were also tuned to find associated galaxies with no constraints on whether the largest galaxy in each group is isolated. The effect of these differences on the anisotropy of the selected population can be seen in Figure 12, where we plot the anisotropy we measure for samples selected using each previous set of criteria versus the fractional contamination from groups as estimated in § 2.3 ($f_{\text{non-dom}}$ in Table 3; note that this is underestimated for criteria that do not include cuts on proximity to the survey edge or on N_{viol} such as SL04, B05, AZPK, APPZ and AB07). The satellites of *isolated* late-type galaxies (on the left) are clustered along the minor axis, while those of late-type galaxies at the centres of groups (on the right) are distributed isotropically. The distribution of satellites around early-types is consistently biased toward the major axis regardless of environment. The results of Y06 and Faltenbacher et al. (2007), whose samples were not selected to be isolated, agree with those on the right side of Figure 12: an isotropic distribution around late-type galaxies, a

major-axis alignment around early-types, and a major-axis alignment of the full sample.

It is particularly informative to compare B05 S3 and ZSFW. These samples have very similar parameters for the isolation and satellite selection criteria, but produce very different results. There are four main differences between the criteria used to select these samples: (1) B05 used $f_{\text{sat}} = 1.0$ while ZSFW imposed no such cut; (2) ZSFW used $N_{\text{viol}} = 0$ while B05 imposed no such cut; (3) B05 imposed no cut on primaries near the survey magnitude limit while ZSFW observed deep enough that all potential bright neighbours were above the magnitude limit; and (4) B05 imposed no cut on proximity to the survey edge while ZSFW observed a large enough area to encompass all prospective bright neighbours. We have systematically varied each of these parameters and analyzed which changes are responsible for the dramatic difference between the results. Variable (2), the cut on N_{viol} , is responsible for almost the entire difference between the samples. The mean disc angle around late-types using the criteria of B05 S3 is 44.1° ; if we impose $N_{\text{viol}} = 0$ then this rises to 47.5° , consistent with the ZSFW sample. On the other hand, variable (1), changing f_{sat} between 1 and ∞ , has no effect whatsoever, and implementing variables (3) and (4),

the cuts on primary magnitude and proximity to the survey edge, only raises the mean to 44.2° . These results could be anticipated from Figure 8, which demonstrated the effects that these parameters have on the observed anisotropy, and emphasise that it is crucial to eliminate spectroscopically-unconfirmed bright neighbours either using a cut on N_{viol} or using photometric redshifts in order to select isolated galaxies.

5 SUMMARY AND DISCUSSION

We summarise the combination of our results with those of previous studies as follows:

- Satellites of isolated disc galaxies lie preferentially perpendicular to the plane of the disc, and the degree of alignment peaks at intermediate radii ($\sim 200\text{--}350 h^{-1} \text{ kpc}$). While satellites beyond $200 h^{-1} \text{ kpc}$ may be aligned preferentially with surrounding large scale filaments, the innermost satellites show no alignment with the LSS.
- Satellites of isolated early-type galaxies lie preferentially along the major axis of the galaxy. The degree of alignment increases slightly for satellites further away from the primary. All satellites show hints of preferential alignment with the surrounding LSS (i.e. filaments).
- Member galaxies within galaxy groups whose BGG is a disc galaxy shown no preferential alignments with respect to the orientation of the BGG.
- Member galaxies within galaxy groups whose BGG is an early-type tend to align with the major axis of the BGG, mirroring the behaviour of the satellites of isolated early-types.
- An alignment between isolated early-type galaxies and the surrounding LSS is detected, but we do not detect any such alignment for isolated late-type galaxies.
- Great care must be taken in order to select truly isolated galaxies and their satellites in galaxy redshift surveys. Unless the region immediately surrounding the primary is devoid of galaxies too large to be considered satellites (*whether or not those galaxies have been observed spectroscopically*), the sample will be dominated by group members rather than isolated galaxies.

These results provide us with the foundations on which we can build our understanding of the mass distribution in and around galaxies. The main result we find is that there is strong evidence in favour of the well known ‘‘Holmberg Effect’’, the preferential alignment of satellite galaxies of isolated spirals in the plane perpendicular to the galactic disc. In contrast, the satellites of isolated early-types tend to cluster around the major axis of their primary. Additionally, we observe that satellites of both early-type and late-type galaxies that have large projected separations from their primary tend to align with the surrounding LSS, and we note a tendency for early-types to orient along the major axis of the surrounding LSS.

These observations raise a number of interesting questions. What can we learn about the role of dynamical effects in driving preferential alignments of satellites? What is the nature of these effects and does it depend on the morphological type of the galaxy? What role is played by the host dark matter halo? What role is played by the

larger scale environment? Our results allow us to begin to address these questions.

The most straightforward interpretation of the preferential alignment of satellites at large projected radii with the surrounding LSS is that this is a signature of the anisotropic infall of satellite galaxies along filaments. This interpretation is favoured by the following observations;

- the mean angle between the projected positions of satellites and the surrounding LSS (i.e. the LSS angle) is similar for both early- and late-type galaxies;
- the alignment is present for *only* the more distant and therefore more recently accreted satellites around late-type primaries; and
- the alignment is distinctive when compared to the alignment of the satellites with respect to their primary. This effect is most marked in systems in which the primary is a late-type galaxy; the satellites of late-type primaries tend to align with the surrounding LSS whereas the primary shows no preferential orientation.

This evidence argues strongly in favour of an origin that is imposed by the larger scale environment rather than one driven by the primary galaxy. In other words, it is improbable that the dynamics of the most recently accreted satellites will be significantly affected by any process internal to the primary’s dark matter halo. This is in agreement with the results of cosmological simulations (Knebe et al. 2004; Zentner et al. 2005; Libeskind et al. 2005).

The relationship between the orientation of a galaxy and its surrounding LSS can be understood in terms of the relationship between the orientation of the galaxy’s dark matter halo and its surrounding LSS *and* the galaxy’s orientation within its dark matter halo. Cosmological N -body simulations predict that dark matter haloes are strongly triaxial systems in the absence of baryons (e.g. Allgood et al. 2006), and these haloes tend to align with their major axes along the large scale filaments and their minor axes perpendicular to filaments (Bailin & Steinmetz 2005).

However, the presence of baryons can have a dramatic effect on the shapes and internal alignments of dark matter haloes, with interesting consequences for the haloes of disc galaxies. A number of studies have shown that cooling baryons at the centre of a dark matter halo tend to circularise the orbits of dark matter particles, modifying the halo’s inner mass profile (e.g. Gustafsson et al. 2006) and reducing the ellipticity of the halo’s isodensity surfaces (e.g. Dubinski 1994; Kazantzidis et al. 2004). Bailin et al. (2005) examined the structure of the host haloes of several disc galaxies that formed in high resolution cosmological N -body hydrodynamical simulations, and discovered that haloes consisted of two distinct regions. The inner halo is flattened along the disk axis, while the orientation of the outer halo is unrelated to that of the inner halo and is unaffected by the presence of the luminous galaxy.

The Bailin et al. (2005) result is interesting because it implies that the major axis of the inner halo around a typical disc galaxy is aligned with the major axis of the light distribution, while the major axis in the outer region is independent of the light but is aligned with the LSS. If satellite galaxies are more common along the halo major axis,

then this “twisting” of the halo should be evident in the distribution of satellites around disc galaxies. This provides a possible explanation for both the absence of a correlation between the orientation of discs and their surrounding LSS and the radial dependence of the satellite-LSS correlation around discs.

In the case of early-type galaxies, the orientation of the galaxy with respect to its dark matter halo has not been studied explicitly in a cosmological context. However, we would expect that the shapes of both their stellar and dark matter components are supported by their anisotropic velocity ellipsoid. Consequently, we would expect that both the galaxy and its dark matter halo will share the same orientation, and therefore the galaxy will tend to align with the surrounding LSS (Bailin & Steinmetz 2005).

How should we interpret the preferential alignments of satellites around isolated early- and late-type galaxies? Can we determine whether the alignments are imprinted by the dynamical effects of the galaxy or the host dark matter halo?

Agustsson & Brainerd (2006), AB07 and Kang et al. (2007) studied the angular distribution of satellite galaxies in cosmological simulations selected according to the criteria of B05, AB07 and Y06 respectively. The orientation of a mock galaxy must be assumed and so these authors explored different assumptions about how primary galaxies are oriented with respect to their dark matter haloes and the larger scale environment. They found that if the primary galaxy is a spheroidal whose principal axes are perfectly aligned with those of its dark matter halo, then satellites in these systems tend to show a major-axis anisotropy that is stronger than observed in groups whose BGG is an early-type galaxy. However, if there is a small offset between the principal axes of the galaxy and its halo, as may arise if the galaxy aligns with the halo’s angular momentum rather than its minor axis, then the anisotropy is of the same order that is observed. Because the alignment of satellites relative to isolated early-types is identical to that seen in galaxy groups whose BGG is an early-type, we may therefore conclude that the principal axes of isolated early-types are reasonably well aligned with those of their dark matter haloes ($\sim 20^\circ$). As we argued above, this is in accord with our expectation that the dynamics of baryons and dark matter in collisionless ellipsoidal systems are similar.

The theoretical situation for galaxy groups whose BGG is a late-type is less clear. If the disc is oriented perpendicular to its halo’s angular momentum, it is simply a special case of an oblate spheroid, and therefore these studies predict that its satellites will exhibit major-axis alignment, contrary to all observations. If, on the other hand, the angular momenta of galaxy discs align with the intermediate axis of the surrounding mass distribution, as seen in the simulations of Navarro et al. (2004), then satellites in these systems show no preferential alignments. This is consistent with the lack of anisotropy detected in groups around late-type BGGs, as probed by most previous observational studies of satellite anisotropy. An alternative explanation for this lack of anisotropy is that groups whose BGG is a disc galaxy are dynamically unrelaxed, in contrast to those groups whose BGG is an early-type (Zabludoff & Mulchaey 1998; Brough et al. 2006). Therefore, it is likely that the members of such groups

are unsuitable as tracers of the dark matter halo or any equilibrium dynamical process.

This leaves open the interpretation of the observed polar alignment of satellites around isolated disc galaxies, which is not predicted by any of the above studies. The persistence of the anisotropy out to $350 h^{-1} \text{ kpc}$ argues against a direct dynamical effect of the disc such as in Peñarrubia et al. (2002); however, an origin that reflects the dynamical effect of a triaxial dark matter halo on the orbits of satellites (e.g. Knebe et al. 2004; Zentner et al. 2005), or an intrinsic bias in the spatial distribution of dark matter subhaloes that host luminous satellites (e.g. Zentner et al. 2005; Libeskind et al. 2005), remains viable. A theoretical analysis that takes into account the dependence of the anisotropy on the selection criteria and the difference between early-type and late-type primaries must be performed to determine whether the observed polar distribution around isolated disc galaxies is determined by the orientation of the halo or if dynamical processes within the halo are important. We are in the process of performing such an analysis (Power et al., in preparation).

ACKNOWLEDGEMENTS

JB thanks Mike Blanton for writing KCORRECT, the SDSS help desk for their help with the Catalog Archive Server, Stéphane Herbert-Fort, Pavel Kroupa and Manuel Metz for useful discussions, and John and Lexi Moustakas for writing the RED IDL cosmological routines. Three-dimensional visualisation was conducted with the S2PLOT programming library (Barnes et al. 2006).

JB acknowledges the financial assistance of the Australian Research Council. CP and BKG gratefully acknowledge the support of the Australian Research Council supported “Commonwealth Cosmology Initiative”, DP 0665574. During the course of this work, PN acknowledges funding from a Zwicky Fellowship at ETH and a PPARC PDRA Fellowship at the IfA. DZ acknowledges support from NASA LTSA award NNG5-GE82G, NSF grant AST-0307482, and a Guggenheim fellowship, and thanks the NYU Physics department and Centre for Cosmology and Particle Physics for their generous support during his sabbatical there.

Funding for the Sloan Digital Sky Survey (SDSS) has been provided by the Alfred P. Sloan Foundation, the Participating Institutions, the National Aeronautics and Space Administration, the National Science Foundation, the U.S. Department of Energy, the Japanese Monbukagakusho, and the Max Planck Society. The SDSS Web site is <http://www.sdss.org/>.

The SDSS is managed by the Astrophysical Research Consortium (ARC) for the Participating Institutions. The Participating Institutions are The University of Chicago, Fermilab, the Institute for Advanced Study, the Japan Participation Group, The Johns Hopkins University, the Korean Scientist Group, Los Alamos National Laboratory, the Max-Planck-Institute for Astronomy (MPIA), the Max-Planck-Institute for Astrophysics (MPA), New Mexico State University, University of Pittsburgh, University of Portsmouth, Princeton University, the United States Naval Observatory, and the University of Washington.

REFERENCES

- Adelman-McCarthy, J. K. et al. 2007, ApJS, submitted
- Agustsson, I., Brainerd, T. G. 2006, ApJ, 650, 550 (AB06)
- . 2007, ApJ, submitted, arXiv:0704.3441 (AB07)
- Allgood, B., Flores, R. A., Primack, J. R., Kravtsov, A. V., Wechsler, R. H., Faltenbacher, A., Bullock, J. S. 2006, MNRAS, 367, 1781
- Argyres, P. C., Groth, E. J., Peebles, P. J. E., Struble, M. F. 1986, AJ, 91, 471
- Azzaro, M., Patiri, S. G., Prada, F., Zentner, A. R. 2007, MNRAS, 376, L43 (APPZ)
- Azzaro, M., Zentner, A. R., Prada, F., Klypin, A. A. 2006, ApJ, 645, 228 (AZPK)
- Bailin, J. et al. 2005, ApJ, 627, L17
- Bailin, J., Steinmetz, M. 2005, ApJ, 627, 647
- Barnes, D. G., Fluke, C. J., Bourke, P. D., Parry, O. T. 2006, Publications of the Astronomical Society of Australia, 23, 82
- Berlind, A. A., Weinberg, D. H. 2002, ApJ, 575, 587
- Binggeli, B. 1982, A&A, 107, 338
- Blanton, M. R. et al. 2003, AJ, 125, 2348
- Brainerd, T. G. 2005, ApJ, 628, L101 (B05)
- Brough, S., Forbes, D. A., Kilborn, V. A., Couch, W. 2006, MNRAS, 370, 1223
- Buote, D. A., Jeltama, T. E., Canizares, C. R., Garmire, G. P. 2002, ApJ, 577, 183
- Chen, J., Kravtsov, A. V., Prada, F., Sheldon, E. S., Klypin, A. A., Blanton, M. R., Brinkmann, J., Thakar, A. R. 2006, ApJ, 647, 86
- Cole, S., Lacey, C. G., Baugh, C. M., Frenk, C. S. 2000, MNRAS, 319, 168
- Colless, M. et al. 2001, MNRAS, 328, 1039
- Conroy, C. et al. 2007, ApJ, 654, 153
- Conroy, C., Wechsler, R. H., Kravtsov, A. V. 2006, ApJ, 647, 201
- de Vaucouleurs, G., de Vaucouleurs, A., Corwin, H. G., Buta, R. J., Paturel, G., Fouque, P. 1991, Third Reference Catalogue of Bright Galaxies (Volume 1-3, XII, 2069 pp. 7 figs.. Springer-Verlag Berlin Heidelberg New York)
- Donoso, E., O'Mill, A., Lambas, D. G. 2006, MNRAS, 369, 479
- Dubinski, J. 1994, ApJ, 431, 617
- Eisenstein, D. J. et al. 2001, AJ, 122, 2267
- Faltenbacher, A., Li, C., Mao, S., van den Bosch, F. C., Yang, X., Jing, Y. P., Pasquali, A., Mo, H. J. 2007, ApJL, in press (arXiv:0704.0674v1)
- Gao, L., White, S. D. M., Jenkins, A., Stoeck, F., Springel, V. 2004, MNRAS, 355, 819
- Gustafsson, M., Fairbairn, M., Sommer-Larsen, J. 2006, Phys. Rev. D, 74, 123522
- Hartwick, F. D. A. 2000, AJ, 119, 2248
- Helmi, A. 2004, ApJ, 610, L97
- Hoekstra, H., Yee, H. K. C., Gladders, M. D. 2004, ApJ, 606, 67
- Holmberg, E. 1969, Arkiv för Astronomi, 5, 305
- Ibata, R., Lewis, G. F., Irwin, M., Totten, E., Quinn, T. 2001, ApJ, 551, 294
- Jenkins, A., Frenk, C. S., White, S. D. M., Colberg, J. M., Cole, S.,+ Evrard, A. E., Couchman, H. M. P., Yoshida, N. 2001, MNRAS, 321, 372
- Johnston, K. V., Law, D. R., Majewski, S. R. 2005, ApJ, 619, 800
- Kang, X., van den Bosch, F. C., Yang, X., Mao, S., Mo, H. J., Li, C., Jing, Y. P. 2007, MNRAS, in press, astro-ph/0701130
- Karachentsev, I. D. et al. 2003, A&A, 398, 479
- Kazantzidis, S., Kravtsov, A. V., Zentner, A. R., Allgood, B., Nagai, D., Moore, B. 2004, ApJ, 611, L73
- Knebe, A., Gill, S. P. D., Gibson, B. K., Lewis, G. F., Ibata, R. A., Dopita, M. A. 2004, ApJ, 603, 7
- Koch, A., Grebel, E. K. 2006, AJ, 131, 1405
- Kroupa, P., Theis, C., Boily, C. M. 2005, A&A, 431, 517
- Lambas, D. G., Groth, E. J., Peebles, P. J. E. 1988, AJ, 95, 996
- Law, D. R., Johnston, K. V., Majewski, S. R. 2005, ApJ, 619, 807
- Libeskind, N. I., Frenk, C. S., Cole, S., Helly, J. C., Jenkins, A., Navarro, J. F., Power, C. 2005, MNRAS, 363, 146
- Lukić, Z., Heitmann, K., Habib, S., Bashinsky, S., Ricker, P. M. 2007, ApJ, submitted, astro-ph/0702360
- Lynden-Bell, D. 1976, MNRAS, 174, 695
- Mandelbaum, R., Hirata, C. M., Broderick, T., Seljak, U., Brinkmann, J. 2006, MNRAS, 370, 1008
- Mandelbaum, R. et al. 2005, MNRAS, 361, 1287
- Martínez-Delgado, D., Gómez-Flechoso, M. Á., Aparicio, A., Carrera, R. 2004, ApJ, 601, 242
- McConnachie, A. W., Irwin, M. J. 2006, MNRAS, 365, 902
- Metz, M., Kroupa, P., Jerjen, H. 2007, MNRAS, 374, 1125
- Muriel, H., Lambas, D. G. 1989, AJ, 98, 1995
- Navarro, J. F., Abadi, M. G., Steinmetz, M. 2004, ApJ, 613, L41
- Norberg, P., Frenk, C. S., Cole, S. 2007, MNRAS, submitted
- Olling, R. P., Merrifield, M. R. 2000, MNRAS, 311, 361
- Palma, C., Majewski, S. R., Johnston, K. V. 2002, ApJ, 564, 736
- Peñarrubia, J., Kroupa, P., Boily, C. M. 2002, MNRAS, 333, 779
- Power, C. 2003, PhD thesis, Durham University
- Prada, F. et al. 2003, ApJ, 598, 260
- Sales, L., Lambas, D. G. 2004, MNRAS, 348, 1236 (SL04)
- Schechter, P. 1976, ApJ, 203, 297
- Schlegel, D. J., Finkbeiner, D. P., Davis, M. 1998, ApJ, 500, 525
- Seljak, U., Zaldarriaga, M. 1996, ApJ, 469, 437
- Sheth, R. K., Tormen, G. 1999, MNRAS, 308, 119
- Simon, J. D., Bolatto, A. D., Leroy, A., Blitz, L., Gates, E. L. 2005, ApJ, 621, 757
- Strauss, M. A. et al. 2002, AJ, 124, 1810
- Trujillo, I., Carretero, C., Patiri, S. G. 2006, ApJ, 640, L111
- van den Bosch, F. C., Norberg, P., Mo, H. J., Yang, X. 2004, MNRAS, 352, 1302
- van den Bosch, F. C., Yang, X., Mo, H. J. 2003, MNRAS, 340, 771
- van den Bosch, F. C., Yang, X., Mo, H. J., Norberg, P. 2005, MNRAS, 356, 1233
- Vincent, R. A., Ryden, B. S. 2005, ApJ, 623, 137
- West, M. J. 1989, ApJ, 347, 610
- Yang, X., Mo, H. J., van den Bosch, F. C. 2003, MNRAS, 339, 1057
- Yang, X., Mo, H. J., Jing, Y. P., van den Bosch, F. C., Chu, Y. 2004, MNRAS, 350, 1153 (Y04)
- Yang, X., van den Bosch, F. C., Mo, H. J., Mao, S., Kang,

- X., Weinmann, S. M., Guo, Y., Jing, Y. P. 2006, MNRAS, 369, 1293 (Y06)
 York, D. G. et al. 2000, AJ, 120, 1579
 Zabludoff, A. I., Mulchaey, J. S. 1998, ApJ, 496, 39
 Zaritsky, D., Smith, R., Frenk, C., White, S. D. M. 1997a, ApJ, 478, 39
 Zaritsky, D., Smith, R., Frenk, C. S., White, S. D. M. 1997b, ApJ, 478, L53 (ZSFW)
 Zentner, A. R., Kravtsov, A. V., Gnedin, O. Y., Klypin, A. A. 2005, ApJ, 629, 219

APPENDIX A: THE CONDITIONAL LUMINOSITY FUNCTION : PARAMETERS

Yang et al. (2003) deduced a functional form for the variation of the mass-to-light ratio with dark matter halo mass by comparing the Sheth & Tormen (1999) dark matter halo mass function with the Schechter luminosity function (Schechter 1976). They noted that the mass-to-light ratio must increase (decrease) with decreasing (increasing) halo mass, and proposed a parameterisation for the variation of the average total mass-to-light ratio with halo mass,

$$\left\langle \frac{M}{L} \right\rangle (M) = \frac{1}{2} \left(\frac{M}{L} \right)_0 \left[\left(\frac{M}{M_1} \right)^{-\gamma_1} + \left(\frac{M}{M_1} \right)^{\gamma_2} \right]. \quad (\text{A1})$$

Here the free parameters correspond to M_1 , the characteristic mass for which the mass-to-light ratio in b_J is equal to $(M/L)_0$, and γ_1 and γ_2 which determine the behaviour at the low- and high-mass ends of the mass function respectively. We follow Yang et al. (2004) (Y04) in adopting $M_1 = 10^{10.94} h^{-1} M_\odot$, $(M/L)_0 = 124 h (M/L)_\odot$ in b_J , $\gamma_1 = 2.02$, and $\gamma_2 = 0.30$.

The characteristic luminosity \tilde{L}^* is parameterised in a similar manner;

$$\frac{M}{\tilde{L}^*} = \frac{1}{2} \left(\frac{M}{L} \right)_0 f(\tilde{\alpha}) \left[\left(\frac{M}{M_1} \right)^{-\gamma_1} + \left(\frac{M}{M_2} \right)^{\gamma_3} \right], \quad (\text{A2})$$

where M_2 is a characteristic mass and γ_3 determines the behaviour at the high-mass end of the mass function; $\tilde{\alpha}$ follows

$$\tilde{\alpha} = \alpha_{15} + \eta \log(M_{15}), \quad (\text{A3})$$

where M_{15} is the mass of the halo in units of $10^{15} h^{-1} M_\odot$ and α_{15} and η are free parameters. We follow Y04 in adopting $M_2 = 10^{12.04} h^{-1} M_\odot$, $\gamma_3 = 0.72$, $\eta = -0.22$, and $\alpha_{15} = -1.1$.

Expression A1 and A2 allow an expression for $\langle L \rangle / \langle M \rangle$ to be derived, from which $\tilde{\Phi}^*$ is deduced;

$$\left\langle \frac{L}{M} \right\rangle (M) = \int_0^\infty \Phi(L|M) \frac{L}{M} dL = \Phi^* \frac{\tilde{L}^*}{M} \Gamma(\alpha + 2) \quad (\text{A4})$$

leads to

$$\tilde{\Phi}^*(M) = \frac{1}{\Gamma(\tilde{\alpha} + 1, 1)} \frac{[(M/M_1)^{-\gamma_1} + (M/M_2)^{\gamma_3}]}{[(M/M_1)^{-\gamma_1} + (M/M_1)^{\gamma_2}]} \quad (\text{A5})$$

Here $\Gamma(x)$ and $\Gamma(x, a)$ are the Gamma and Incomplete Gamma functions respectively; formally these are expressed as

$$\Gamma(x) = \int_0^\infty t^{x-1} \exp(-t) dt \quad (\text{A6})$$

and

$$\Gamma(x, a) = \int_a^\infty t^{x-1} \exp(-t) dt \quad (\text{A7})$$

We note that Y04 denote the average mass-to-light ratio by $\langle M/L \rangle$ (see their Equation 2). We prefer $\langle M \rangle / \langle L \rangle$ because the meaning is clear – the average luminosity associated with a halo of mass M is $\langle L \rangle$ and so the average mass-to-light ratio is $\langle M \rangle / \langle L \rangle$. If we adopt $\langle M/L \rangle$, this means that

$$\left\langle \frac{M}{L} \right\rangle (M) = \int_0^\infty \Phi(L|M) \frac{M}{L} dL = \Phi^* \frac{M}{\tilde{L}^*} \Gamma(\tilde{\alpha}). \quad (\text{A8})$$

This produces an expression for $\tilde{\Phi}^*$ that is quite different from Equation A5, and which does not recover the correct behaviour of quantities such as $\langle N \rangle (M)$.

Having deduced the form of $\tilde{\Phi}^*$, we can compute the “conditional luminosity function” $\Phi(L|M)$,

$$\Phi(L|M) dL = \frac{\tilde{\Phi}^*}{\tilde{L}^*} \left(\frac{L}{\tilde{L}^*} \right)^{\tilde{\alpha}} \exp(-L/\tilde{L}^*) dL.$$

The upper left-hand panels of Figure A1 show how \tilde{L}^* and $\tilde{\Phi}^*$ vary with halo mass, while the right-hand panel shows the variation of $\Phi(L|M)$ with luminosity at a fixed halo mass for the Y04 choice of 2dFGRS parameters.

APPENDIX B: POPULATING DARK MATTER HALOES WITH GALAXIES : DETAILS

We perform a suite of cosmological N -body simulations and constructed catalogues of dark matter haloes at $z=0$. Dark matter haloes are identified using a *friends-of-friends* (FOF) algorithm with a linking length of $b = 0.2$ times the mean interparticle separation. For each of the groups identified in this way we compute the virial mass M_{180} , defined as the mass of the spherical overdensity that is 180 times the critical density of the Universe at $z=0$. In the following discussion, we define a halo’s mass M to be its virial mass M_{180} rather than M_{FOF} , the mass of the FOF group; this is required by the Y04 prescription.

The minimum halo mass M_{min} that is “reliably” recovered in each of the simulations governs the minimum luminosity, L_{min} , that is used in constructing the mock catalogues. L_{min} defines the threshold luminosity fainter than which there are no galaxies. M_{min} is the halo mass above which we expect the mass function to be unaffected by finite numerical resolution; below this threshold the number density of haloes tends to be suppressed relative to the number density they would have in the limit of infinite numerical resolution. Previous studies have examined how the mass function is affected by finite mass and force resolution, time-stepping accuracy and starting redshift, as well as the influence of the group-finding algorithm used to identify dark matter haloes (e.g. Jenkins et al. 2001; Lukić et al. 2007). Jenkins et al. (2001) performed careful convergence tests and found that mass functions constructed from FOF groups are adversely affected by numerical effects below a halo mass equivalent to ~ 20 particles. In this work we adopt a more conservative lower mass limit of 50 particles, to ensure that the mass function of haloes in higher density re-

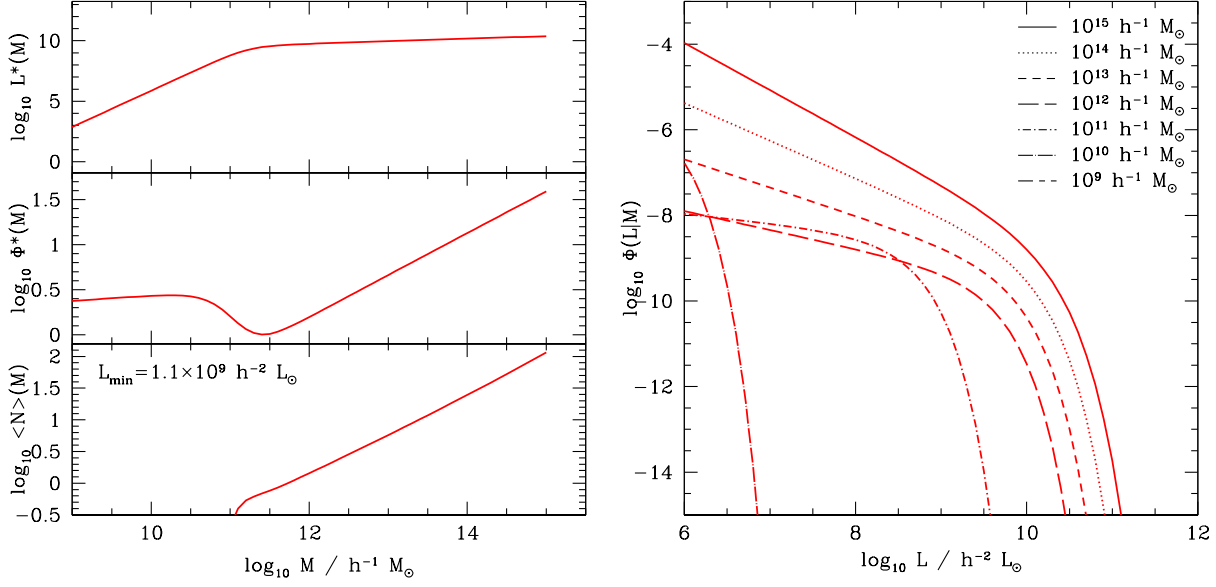


Figure A1. (LEFT) Variation of the conditional luminosity function parameters \tilde{L}^* (upper panel) and $\tilde{\Phi}^*$ (middle panel), and the halo occupation number $\langle N \rangle(M)$ (bottom panel) with halo mass. We adopt the Y04 choice of 2dFGRS parameters and a minimum luminosity $L_{\min} = 1.1 \times 10^9 h^{-2} L_{\odot}$. (RIGHT) Variation of the conditional luminosity function with luminosity at fixed halo masses, for the Y04 parameters.

gions is converged (see Chapter 3 of Power 2003); this gives $M_{\min} = 50 m_{\text{part}}$ in Table 2.

Having determined M_{\min} , we estimate L_{\min} using the “conditional probability distribution” $P(M|L)$ (see right panel of Figure 1, Y04). L_{\min} is a critical parameter because it fixes the halo occupation number, the average number of galaxies per halo of mass M ;

$$\langle N \rangle(M) = \tilde{\Phi}^* \Gamma(\tilde{\alpha} + 1, L_{\min}/\tilde{L}^*). \quad (\text{B1})$$

The variation of $\langle N \rangle(M)$ with halo mass for the Y04 2dFGRS parameters and $L_{\min} = 1.1 \times 10^9 h^{-2} L_{\odot}$ is shown in the bottom left-hand panel of Figure A1. This L_{\min} is appropriate for the M_{\min} in the mock catalogues A to E.

Note the important role played by the ratio L_{\min}/\tilde{L}^* in Equation B1, which controls the number of galaxies per halo. At fixed L_{\min} it increases dramatically as halo mass decreases, leading to low mass haloes containing one “central” galaxy at most, and as L_{\min} decreases, the number of galaxies per halo increases. The number of galaxies per halo of mass M is Poisson distributed with a mean of $\langle N \rangle(M)$.

We note also that Yang et al. (2003) introduced a “hard” lower mass cut-off of $M_{\min} = 10^9 h^{-1} M_{\odot}$ below which haloes cannot host galaxies – galaxy formation is suppressed in these haloes following cosmological reionisation.

Having determined the number of galaxies hosted by a halo, we must assign luminosities. We follow Y04 and give special status to the central galaxy by assuming that it is the brightest in the halo, with an average luminosity

$$\langle L_c \rangle = \tilde{\Phi}^* \tilde{L}^* \Gamma(\tilde{\alpha} + 2, L_1/\tilde{L}^*). \quad (\text{B2})$$

The luminosity L_1 is a function of halo mass and is chosen such that

$$\tilde{\Phi}^* \Gamma(\tilde{\alpha} + 1, L_1/\tilde{L}^*) = 1; \quad (\text{B3})$$

when choosing the central galaxy luminosity, we assume that L_c is a random variable drawn from $\Phi(L|M)$ for the range of luminosities $L > L_1$. The remaining $N - 1$ galaxies within the halo are assigned luminosities in the range $L_{\min} < L < L_1$, drawn at random from the luminosity function (the “intermediate” approach of Y04).

The penultimate step involves assigning morphological types to each mock galaxy; this is done by defining a function $f_{\text{late}}(L, M)$ that specifies the fraction of galaxies with luminosity L in haloes of mass M that are late-type. This function can be expressed as the product of functions,

$$f_{\text{late}}(L, M) = g(L)h(M)q(L, M), \quad (\text{B4})$$

where

$$q(L, M) = \begin{cases} 1 & \text{if } g(L)h(M) \leq 1 \\ \frac{1}{g(L)h(M)} & \text{if } g(L)h(M) > 1 \end{cases}, \quad (\text{B5})$$

$$g(L) = \frac{\hat{\Phi}_{\text{late}}(L)}{\hat{\Phi}(L)} \frac{\int_0^\infty \Phi(L|M)n(M)dM}{\int_0^\infty \Phi(L|M)h(M)n(M)dM}, \quad (\text{B6})$$

and

$$h(M) = \max \left(0, \min \left[1, \left(\frac{\log(M/M_a)}{\log(M_b/M_a)} \right) \right] \right). \quad (\text{B7})$$

Here $n(M)$ is the halo mass function (Sheth & Tormen 1999); $\hat{\Phi}_{\text{late}}(L)$ and $\hat{\Phi}(L)$ correspond to the *observed* luminosity functions of the late-type and entire galaxy samples respectively; and M_a and M_b are free parameters defined as the masses at which $h(M)$ takes on the values 0 and 1 respectively. van den Bosch et al. (2003) demonstrated that this parameterisation allowed the galaxy population to be split into early- and late-types such that the respective

luminosity functions and clustering properties could be recovered. We follow Y04 in adopting $M_a = 10^{17.26} h^{-1} M_\odot$ and $M_b = 10^{10.86} h^{-1} M_\odot$. Formally we assign morphological type by drawing a random number R that is uniformly distributed between $[0, 1]$ and comparing it to $f_{\text{late}}(L, M)$. If $R < f_{\text{late}}(L, M)$, the galaxy is designated late-type, otherwise it is early-type.

The final step involves assigning phase space coordinates (i.e. positions and velocities) to each of the N galaxies within the halo. The brightest central galaxy is associated with the most bound particle of the halo and is assigned its position and velocity. The remaining $N-1$ galaxies can be treated in a variety of ways. For the purposes of this study, in which our main concern is testing the reliability of our selection criteria, we follow Y04 in randomly sampling dark matter particles from the FOF group (their “FOF approach”). More sophisticated approaches, in which we explicitly track the merging history of individual haloes, will be essential for future work, especially with regards to kinematics (Power et al., in preparation).

APPENDIX C: GALAXY CLASSIFICATION

Many properties of galaxies are bimodal. In order to classify galaxies into early-type spheroid-dominated galaxies and late-type disc-dominated galaxies, we focus on the following properties:

(i) Location on the colour-magnitude diagram (CMD). Figure C1a shows the distribution of spectroscopic galaxies from SDSS DR5 in the $^{0.1}(g-r)$ versus $M_r - 5 \log h$ plane. The red sequence and blue cloud are clearly distinguishable. We draw a line separating the populations at

$$^{0.1}(g-r) = 0.78 - 0.0325(M_r - 5 \log h + 19), \quad (\text{C1})$$

shown as the solid line. Panel (b) shows a histogram of the difference between $^{0.1}(g-r)$ and the line separating the populations and shows the bimodality clearly.

(ii) Spectroscopic Principal Component Analysis (PCA) eClass parameter. Figure C1c shows the distribution of eClass for all spectroscopic galaxies in SDSS DR5.

(iii) The concentration of the light profile, C , defined as

$$C = \frac{R_{90}}{R_{50}}, \quad (\text{C2})$$

where R_{50} and R_{90} are the r -band Petrosian radii encompassing 50% and 90% of the flux respectively. Figure C1d shows the distribution of C for all spectroscopic galaxies in SDSS DR5.

It should be noted that these measurements are completely independent: the CMD location is based on global photometry, the PCA analysis is based on spectroscopy, and the Petrosian concentration is based on the distribution of the light profile.

We draw a vertical line on each histogram separating the population into early- and late-type galaxies. Because the populations overlap for each parameter, the separation is not perfectly clean. The bimodality can be enhanced by combining several pieces of information. In particular, we use a linear combination of the above parameters to determine a separation parameter s_{all} :

Table C1. Galaxy Classification Parameters

Method	w_i	δ_i
CMD	1.0	0.3
eClass	0.4	0.2
C	0.5	0.7

$$s_{\text{all}} = \frac{\sum_i w_i s_i}{\sum_i w_i}, \quad (\text{C3})$$

where each individual parameter i is given a weight w_i based on the degree of bimodality its individual distribution shows, and the individual separation parameters are

$$s_{\text{CMD}} = \frac{^{0.1}(g-r) + 0.0325(M_r - 5 \log h + 19) - 0.78}{\delta_{\text{CMD}}}, \quad (\text{C4})$$

$$s_{\text{eClass}} = -\frac{\text{eClass} + 0.07}{\delta_{\text{eClass}}}, \quad (\text{C5})$$

$$s_C = \frac{C - 2.6}{\delta_C}, \text{ and} \quad (\text{C6})$$

$$s_{\text{deV}} = \frac{f_{\text{deV}} - 0.6}{\delta_{\text{deV}}}. \quad (\text{C7})$$

The δ_i values give the intrinsic width between the peaks of the distribution. Although the weights w_i and widths δ_i are completely degenerate through the combination w_i/δ_i , we prefer to make explicit the difference between the objectively-determined width of the distribution from the more subjective weight. The weights w_i and widths δ_i are given in Table C1. The distribution of s_{all} is shown in Figure C1e; the bimodality is indeed enhanced compared to the distribution in any individual parameter. We define galaxies with $s_{\text{all}} > 0$ as early-types and $s_{\text{all}} < 0$ as late-types. The distribution of the other parameters for early and late-types defined using s_{all} are shown as the coloured/dashed and dotted histograms in Figure C1.

The s_{all} criterion can be equivalently considered as a plane in the three-dimensional CMD location-eClass- C parameter space. Figure C1f contains an image and online animation of how this plane successfully separates the locus of early-type galaxies in this parameter space from the region occupied by late-type galaxies.

We use the s_{all} classification as our fiducial classification. However, given the qualitative difference between our results for the early- and late-type subpopulations, it is important to confirm that the difference seen is not an artefact of the galaxy classification scheme. We therefore split the primary sample into early- and late-type galaxies using each individual parameter described above and plot the results in Figure C2. The mean disc angle and KS test probability that each sample is drawn from an isotropic distribution are also given. The planar distribution around early-type galaxies and the polar distribution around late-type galaxies is seen using every method. Therefore, although the magnitude of the measured anisotropy varies at a $\sim 1\sigma$ level, the detected anisotropy cannot be simply a galaxy classification artefact: satellites of early-type and late-type galaxies have intrinsically opposite alignments. It is interesting that the difference between the samples is stronger when using classification schemes based on the stellar populations than when using a scheme based on morphology.

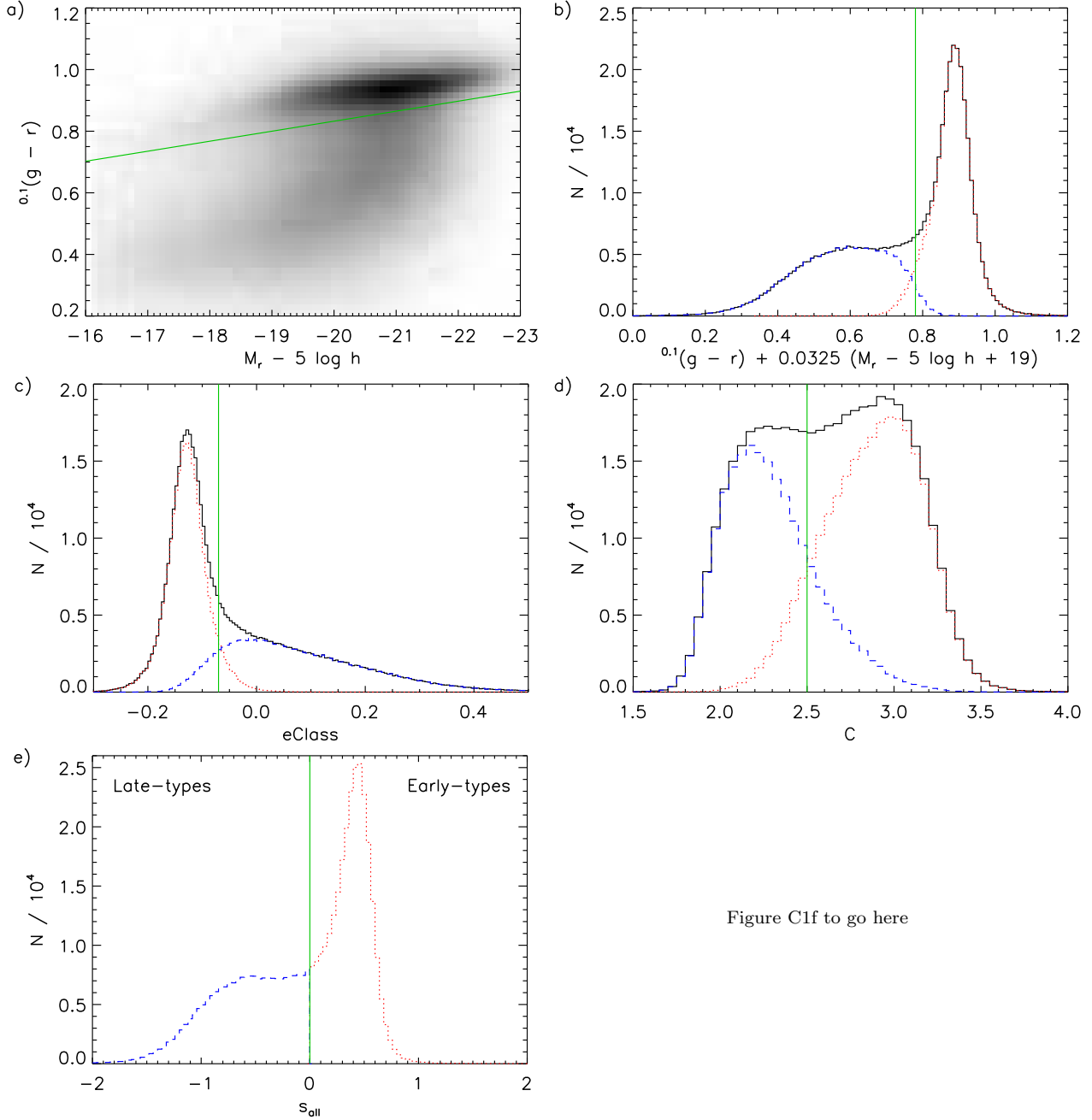


Figure C1f to go here

Figure C1. (a) $^{0.1}(g-r)$ versus M_r colour-magnitude diagram (CMD) for all spectroscopic galaxies from SDSS DR5. The red sequence and blue cloud are clearly visible. The line denotes the separation drawn between the early- and late-types. (b) Histogram of $^{0.1}(g-r)$ scaled by its absolute magnitude, normalised to $M_r - 5 \log h = -19$. The vertical line denotes the CMD-based galaxy classification and is identical to the line in panel (a). In all panels, the red/dotted (blue/dashed) histograms denote galaxies classified as early-type (late-type) based on the s_{all} parameter. (c) Histogram of spectroscopic PCA eClass parameters. The vertical line denotes the eClass-based galaxy classification. (d) Histogram of Petrosian concentration C parameters. The vertical line denotes the C -based galaxy classification. (e) Histogram of s_{all} parameters. The vertical line denotes the s_{all} -based galaxy classification. (f) Image of the density of galaxies in the three-dimensional CMD location-eClass- C parameter space. The plane denotes the separation between early- and late-type galaxies defined by $s_{\text{all}} = 0$. The online version of this article contains a 3D animation of this graphic from a range of viewpoints.

APPENDIX D: ANGULAR DISTRIBUTION OF SATELLITES IN THE MOCK CATALOGUES

To confirm that our measurement of an anisotropic distribution of satellite galaxies is due to an intrinsic anisotropy rather than an artefact of our method, we have performed an identical analysis on the mock catalogues, whose satellite

distributions are, by construction, isotropic. We use mock catalogues generated from the five independent $100 h^{-1} \text{ Mpc}$ simulations in order to account for cosmic variance. The distributions are plotted in Figure D1 and the statistical measures of anisotropy are listed in Table D1.

The level of anisotropy that we measure from

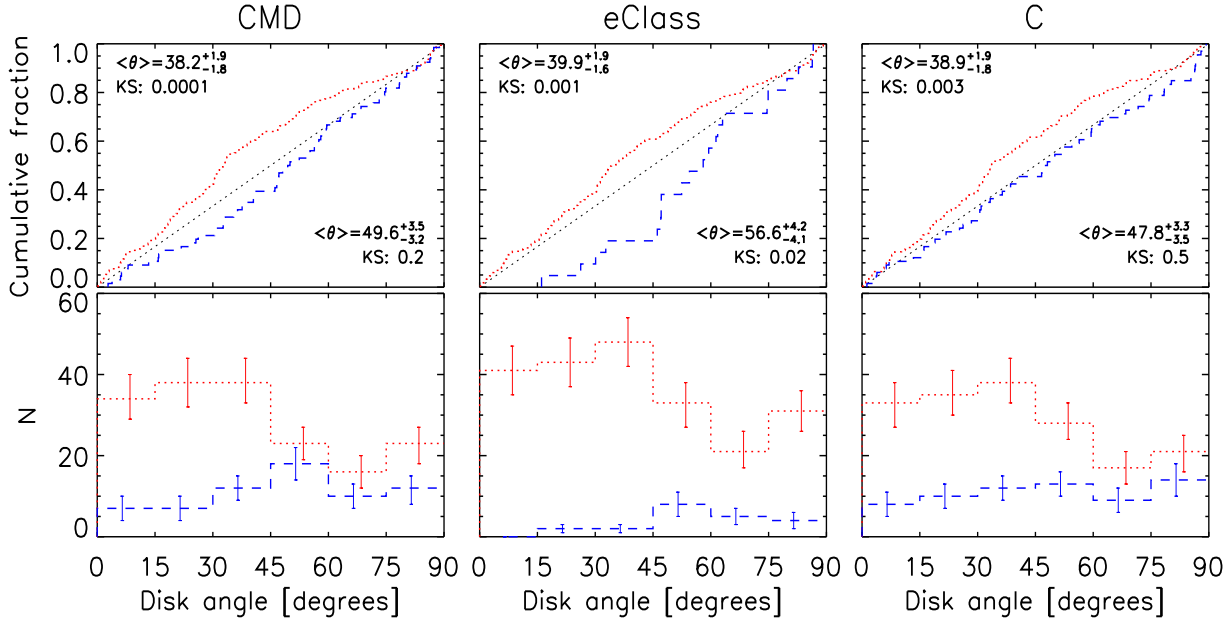


Figure C2. Cumulative (*top panels*) and differential (*bottom panels*) distributions of satellite disc angles of primary galaxies classified using the following schemes (left to right): CMD, spectroscopic eClass parameter, and Petrosian concentration parameter C . Colours/line styles are as in Figure 4. Mean disc angles and KS test probabilities that the samples are drawn from a uniform distribution are given in the top-left (bottom-right) corners of the cumulative plots for the early-type (late-type) samples.

isotropically-distributed satellites in the mock catalogues is small. Even when the isotropic KS test probabilities in the mock samples are low, the deviations are not systematic: the mean disc angle almost always deviates from 45° by less than 2° and a polar fraction that never deviates from 0.5 by more than 4%. These are much smaller than the anisotropies that we detect in the observational sample, confirming that neither our detection of polar alignment around late-types nor our detection of major-axis alignment around early-types can be explained by intrinsically isotropically distributed satellites.

APPENDIX E: DETERMINATION OF THE LARGE SCALE STRUCTURE AXIS

We determine the PA of the large scale structure around each primary galaxy by diagonalising the moment of inertia tensor of the projected positions of all spectroscopic galaxies with projected radii of between 1000 and $3000 h^{-1}$ kpc, and with velocities that differ from that of the primary by no more than 400 km s^{-1} .

We have used the mock catalogues to confirm that this procedure reliably recovers the three-dimensional PA of the LSS surrounding the primary. We have taken the known three-dimensional positions of all haloes within a spherical volume of $3000 h^{-1}$ kpc around the halo of each primary galaxy in the mock catalogues, constructed and diagonalized their inertia tensor, and projected the major axis onto the plane of the sky. The PA of this axis is then compared to the two-dimensional PA inferred from the “observed” galaxies in the mock catalogues. The cumulative distribution of the misalignment between the PA determined using 3D positions and that inferred from the 2D observables is plotted in

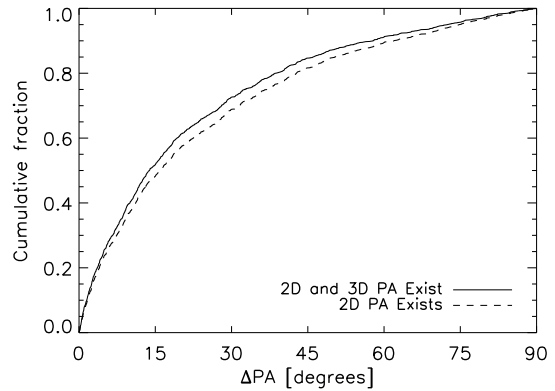
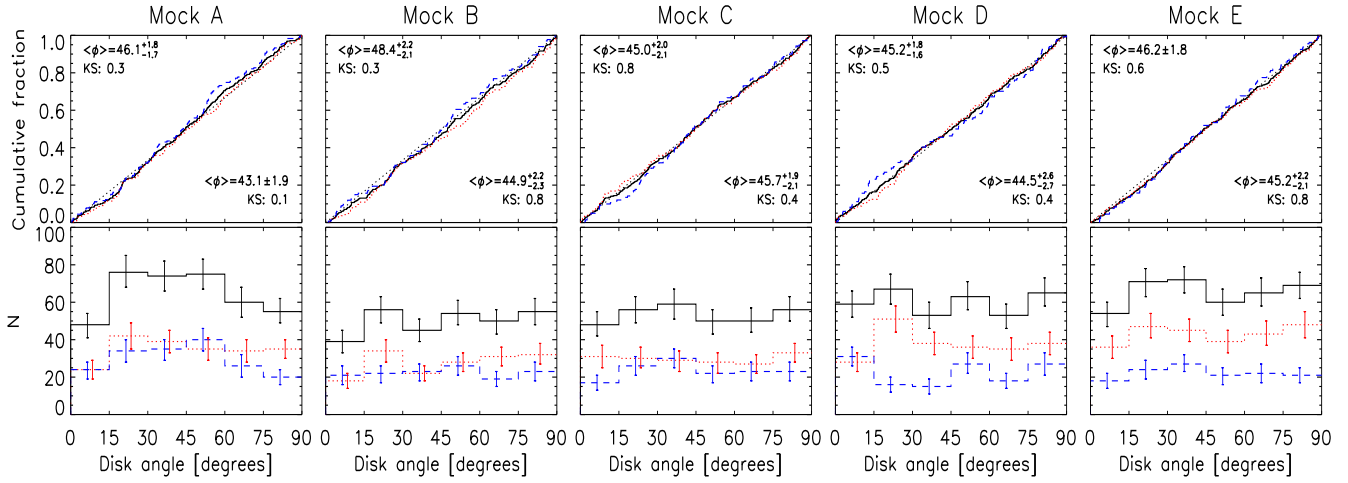


Figure E1. Cumulative distribution of the difference between the PA of the LSS measured around isolated mock galaxies using the “observed” 2D galaxy positions and redshifts versus that measured using the known three-dimensional positions of surrounding haloes. The solid line indicates galaxies for which both the 2D and 3D PA is well-defined, while the dashed line also includes haloes for which only the 2D PA is well-defined.

Figure E1. To improve the statistics, we have included in this plot all galaxies that match the isolation criteria, regardless of whether they have satellites; however, the results are consistent if we restrict the sample to just those with satellites. The solid line indicates the relative alignment when both the 3D LSS PA and the inferred 2D are well-defined (i.e. that contain galaxies within the defining sphere or cylinder), and has a median misalignment of 13.8° . A small fraction of galaxies have well-defined 2D LSS PAs, and would therefore be included in the observational analysis, but no well-defined 3D LSS axis because none of the galaxies that lie within the

Table D1. Anisotropy of Satellites in Mock Catalogues

Parameter	Mock A	Mock B	Mock C	Mock D	Mock E
Full sample:					
KS probability	0.28	0.41	0.95	0.94	0.65
Mean disc angle [°]	$44.7^{+1.4}_{-1.2}$	46.8 ± 1.5	45.3 ± 1.5	$44.9^{+1.5}_{-1.4}$	$45.9^{+1.5}_{-1.4}$
Median disc angle [°]	$44.7^{+2.1}_{-2.0}$	$47.4^{+1.7}_{-2.2}$	$44.4^{+2.9}_{-1.7}$	$45.4^{+2.5}_{-2.7}$	$44.1^{+3.0}_{-1.6}$
Polar fraction	0.49 ± 0.03	0.53 ± 0.03	0.49 ± 0.03	0.50 ± 0.03	0.50 ± 0.03
Early-type primaries:					
KS probability	0.30	0.33	0.76	0.46	0.64
Mean disc angle [°]	$46.1^{+2.0}_{-1.7}$	48.4 ± 2.2	$45.0^{+2.2}_{-2.2}$	45.2 ± 1.7	$46.2^{+1.8}_{-1.7}$
Median disc angle [°]	$44.9^{+4.2}_{-1.9}$	$48.8^{+5.8}_{-1.4}$	$44.8^{+3.2}_{-2.1}$	$44.0^{+3.4}_{-1.8}$	$45.2^{+3.5}_{-3.5}$
Polar fraction	$0.50^{+0.03}_{-0.04}$	0.55 ± 0.04	0.49 ± 0.04	0.48 ± 0.03	0.50 ± 0.03
Late-type primaries:					
KS probability	0.10	0.83	0.45	0.40	0.80
Mean disc angle [°]	$43.1^{+2.0}_{-1.8}$	$44.9^{+2.3}_{-2.2}$	$45.7^{+2.0}_{-2.2}$	$44.5^{+2.6}_{-2.1}$	45.2 ± 2.2
Median disc angle [°]	$43.7^{+2.4}_{-2.7}$	$45.2^{+2.9}_{-2.2}$	$43.7^{+4.1}_{-3.2}$	$47.9^{+5.1}_{-9.4}$	$43.4^{+6.6}_{-4.0}$
Polar fraction	0.48 ± 0.04	0.51 ± 0.04	$0.48^{+0.5}_{-0.4}$	0.54 ± 0.05	0.48 ± 0.05


Figure D1. Cumulative (*top panels*) and differential (*bottom panels*) distributions of satellite disc angles in the five mock catalogues. Colours/line styles are as in Figure 4. Mean disc angles and KS test probabilities that the samples are drawn from a uniform distribution are given in the top-left (bottom-right) corners of the cumulative plots for the early-type (late-type) samples.

redshift-space cylinder lie within the 3D sphere. We account for these cases by assuming that their intrinsic 3D LSS PAs are isotropically distributed and indicate the alignment of the full sample including them as the dashed line in Figure E1. Half of the LSS PAs are aligned to within 15.8° ; therefore, this procedure successfully recovers the PA of the LSS.